Probing Membrane Catalyzed Apelin-Receptor Interactions by Fluorescence Spectroscopy

by

Robin Elisabeth Patterson

Submitted in partial fulfilment of the requirements
for the degree of Master of Science

at

Dalhousie University
Halifax, Nova Scotia
December 2015

Table of Contents

List of Tables

List of Figures

Abstract

Apelin is a peptidic hormone that activates the class A G-protein-coupled apelin receptor. Apelin is found in several bioactive isoforms in the body, ranging from 13 to 55 amino acids in length. Only the C-terminal 12 amino acids are required for bioactivity. Apelin-17 has previously been shown to bind to micelles of anionic detergents, undergoing a membrane-induced structural transition. It has been theorized that a peptide-membrane interaction and the resulting conformational changes are necessary for peptide recognition by the receptor, while also serving to increase local concentration of the ligand in what is known as the membrane catalysis theory. Here, a method is described for conjugating both synthetic and recombinant apelin to fluorescent probes. These fluorescently-labelled peptides were then used in fluorescence experiments to test for membrane-interaction, as required by the membrane catalysis theory. It was found that all three isoforms of apelin interact favourably with both anionic and zwitterionic detergents, as indicated by the calculated *Py* values. Förster resonance energy transfer (FRET) experiments were performed with fluorescently-labelled apelin-17 to native tryptophan in a fragment of the apelin receptor to both localize the ligand-receptor binding interface and to quantify the peptide-receptor interaction.

List of Abbreviations and Symbols Used

ε: molar extinction coefficient

λ: wavelength

τ: fluorescence lifetime

A: acceptor

AR: apelin receptor

CD: circular dichroism

CMC: critical micelle concentration

D: donor

DMF: dimethylformamide

DPC: dodecylphosphocholine

DTT: dithiothrietol

EC_{50}: half-maximal effective concentration

EDTA: ethylenediaminetetraacetic acid

ERK: extracellular signal-regulated kinase

FP: fluorescent protein

FRET: Förster Resonance Energy Transfer

GFP: green fluorescent protein

GPCR: G-protein-coupled receptor

HEK: human embryonic kidney

HIV: human immunodeficiency virus

HOMO: highest occupied molecular orbital

IPTG: isopropyl β-D-1-thiogalactopyranoside

LB: lysogeny broth

LPPG: 1-palmitoyl-2-hydroxy-*sn*-glycero-3-[phospho-*rac*-(1-glycerol)]

LUMO: lowest unoccupied molecular orbital

NMR: nuclear magnetic resonance

NPM: *N*-(1-pyrenyl)maleimide

NTA: nitrilotriacetic acid

OD_{600}: optical density at 600 nm

pERK: phosphorylated extracellular signal-regulated kinase

PMT: photomultiplier tube

POI: protein of interest

Py-Cys-apelin: Cys-apelin modified with *N*-(1-pyrenyl)maleimide at the N-terminus

Py-mercaptoethanol: *N*-(1-pyrenyl)maleimide conjugated to mercaptoethanol

R_0: Förster distance

RP-HPLC: reversed-phase high performance liquid chromatography

SDS: sodium dodecyl sulphate

SEM: standard error of the mean

SUMO: small ubiquitin-like modifier protein

TFA: trifluoroacetic acid

TM: transmembrane

UV: ultraviolet

WT: wild-type

Acknowledgements

Firstly, I would like to thank my supervisor, Dr. Jan K. Rainey, for all of his help and guidance throughout my graduate degree. Jan took me on as a former chemistry student who had never taken a biochemistry class before, and he has been endlessly patient and supportive as I found my feet in the world of structural biology. Jan has allowed me so much freedom with the direction of my project and the techniques that I wanted to learn. I have been exposed to such a range of methods, from fluorescence spectroscopy and NMR, to cell culturing and protein expression. Jan has also encouraged me to participate in several conferences and facilitated this participation. These experiences have expanded both my skill-set and my perspective as a scientist and I'm very grateful to him for these opportunities, as well as everything else.

I would also like to thank all of the members of the Rainey lab, past and present, who have helped me with my research every step along the way, and who created a welcoming and fun atmosphere to work in each day. In particular: Bruce Stewart, Dr. Aditya Pandey, Dr. Marie-Laurence Tremblay, Nigel Chapman, Kyungsoo Shin, Nathan Weatherbee-Martin, Sara Sparavalo, Danielle LeBlanc, Dr. Lingling Xu, and Dr. Muzaddid Sarker. Plus, everyone else in the Rainey lab and the Biochemistry Department who helped make my experience in graduate school truly enjoyable.

I would like to thank my committee members, Dr. Roy Duncan and Dr. Stephen Bearne for their encouragement and ideas over the last two years, as well as the staff in the Biochemistry Department office, in particular Roisin McDevitt, for all the of the non-science related help and support.

Finally, I would like to thank my family: Mom, Dad, Meredith, Nana, and Simon. You have kept me sane and always make me feel like I can do anything.

Thank you.

Chapter 1: Introduction

1.1. Physiological Relevance

Apelin is a small, basic, peptidic hormone that activates a class A G-protein-coupled receptor (GPCR): the apelin receptor (AR). GPCRs are a large family of receptors that are distinguished by their seven transmembrane domains (1). Nearly 30% of all United States Food and Drug Administration-approved drugs target a member of the GPCR family (2). Apelin has been shown to be a potent inotropic agent (3), and is found at high concentrations in patients suffering from chronic heart failure (4). Based on the positioning of dibasic residues in the proprotein precursor, proapelin, it was hypothesized that there were three naturally-occurring bioactive isoforms of apelin: apelin-13, apelin-17 and apelin-36 (nomenclature based on the number of C-terminal residues retained; Figure 1.1); and, indeed, it was proven that synthetic apelin-13, -17, and -36 all activate the AR (5, 6). It has been shown that it is the last 12 C-terminal residues that are essential for receptor activation (7-9). In further support of the hypothesis that dibasic sites are key, previous work in the Rainey lab demonstrates that apelin-13 is specifically enzymatically produced from the 55 amino acid proapelin precursor protein by the proprotein convertase PCSK3/furin (10).

The AR is expressed in various tissues throughout the body, particularly in cardiac and vascular tissues (11), as well as in the central nervous system (12). The apelinergic system has been implicated in obesity and diabetes (13), as well as human immunodeficiency virus (14) and cognitive memory processes (15). Consequently, apelin and the AR have the potential to be a highly desirable drug target, and structural characterization is crucial to further understanding of the apelinergic system.

1.2. Structural Studies of Apelin and the Apelin Receptor

The Rainey lab has used nuclear magnetic resonance (NMR) spectroscopy to solve the structure of apelin-17 in solution at 35 °C and 5 °C (16). These structures indicate converged conformation in residues R6 to L9 (Figure 1.1-1.2). This structuring became further converged at 5 °C in comparison to 35 °C. These findings could indicate that these four residues (RPRL) are involved in ligand-receptor binding, as lower temperature measurements allow for sampling of enthalpically favoured but entropically disfavoured conformations and it has been shown that low temperature ligand structures can correspond to the bound structures (17). Identification of the RPRL motif as a structured region, and therefore likely site of receptor interaction, is also corroborated by the fact that these residues are highly sensitive to alanine substitution (7, 8). Recent studies have also specifically targeted this region, showing that it forms a well-defined β-turn that is necessary for receptor binding (18). Furthermore, the N-terminal region of the AR has been shown to be essential for activity using alanine scanning and truncation studies, with a pair of acidic residues having been shown to be particularly important (19). Therefore, it is plausible that the cationic RPRL residues might interact favourably with this region.

The structure of apelin-17 in the presence of sodium dodecyl sulfate (SDS) micelles has also been solved using NMR spectroscopy (20). Langelaan and Rainey first showed using circular dichroism (CD) spectropolarimetry that upon the addition of SDS micelles, the spectra of apelin-12 and apelin-17 imply induction of some α-helical structuring by the micelles. The NMR structure shows that apelin interacts with the surface of anionic SDS micelles and forms a converged structure from R6 to K12, which includes the RPRL region, with β-turn initiation between R6-L9 and at S10 (Figure 1.1 and 1.3) (20). Apelin-17 also became highly structured in the M15 to F17 region upon interaction with micelles, although

this region does not directly associate with the micelle surface. Structuring of this nature which is induced by interaction with membrane-mimetic micelles, clearly differing from that in buffer (Figure 1.2 vs. Figure 1.3), may be indicative of a receptor binding mechanism that includes catalysis by the cell membrane, further discussed in Section 1.3.

While solving the structure of the full-length AR is an ongoing project, some valuable insight into structure and binding has been provided by studying AR55, the first 55 residues of the AR corresponding to the N-terminus and first transmembrane domain (Figure 1.4). The structure of AR55 in dodecylphosphocholine (DPC) micelles has been solved by Langelaan *et al.* using NMR spectroscopy (21). The structure shows that the N-terminal tail is highly disordered, except for an α-helix from D14 to K25 that contains two key residues, E20 and D23 (Figure 1.4-1.5), previously shown to be essential for receptor activation (19). In the α-helix, E20 and D23 are found just ~9 Å apart on the same face of the helix and in close proximity to the membrane, forming an anionic "patch" that is a likely target for the highly cationic apelin, particularly the structured RPRL motif.

The combination of apelin-17 and AR55 structural studies has allowed for proposing of a potential mechanism by which apelin binds to and activates the AR. It has been proposed that apelin may interact at the anionic patch, an interaction that is facilitated by the cell membrane, after which the apelin-bound but disordered N-terminal domain of AR follows a conformational excursion (or "fly-casting" (22)) mechanism, which facilitates the insertion of the mostly hydrophobic C-terminal region of apelin into the AR transmembrane (TM) bundle and induces activation (21). Insertion into the TM bundle has previously been proposed by Iturrioz *et al.* (23), and this mechanism as a whole is facilitated by an interaction between apelin and the cell membrane, following the membrane catalysis theory, discussed below.

1.3. Membrane Catalysis Theory

The membrane catalysis theory (reviewed in (24)) proposes a mechanism whereby some peptides or proteins may interact with the cell membrane prior to recognition by their cognate receptor. The interaction between ligand and membrane can be either hydrophobic or electrostatic in nature (24). The theory was put forth by Sargent and Schwyzer in 1986, where they described a mechanism for ligand-receptor interactions catalyzed by the lipid membrane (25). The first argument of the theory is that hormone receptors, such as GPCRs, occupy only a very small fraction of the total area of the cell membrane surface. Therefore, as a ligand approaches a cell, it is much more likely that the ligand will find and interact with the cell membrane rather than directly with its cognate receptor. The theory also suggests that many ligand molecules can interact with the cell membrane, effectively increasing the local concentration of the ligand and further increasing the likelihood of randomly interacting with the receptor. Upon binding to the membrane, the ligand may undergo conformational changes, as observed for apelin-17 (20), and these changes may correspond to a conformation that is more favourable for receptor recognition. The membrane works as a catalyst in this theory by reducing the energy barrier for bringing together a peptide and its cognate receptor in a conformation in which the ligand can be recognized and induce activation (25).

1.4. Rationale and Objectives

In order to further examine the membrane catalysis theory and its contribution to apelin-receptor interactions, the first objective of this work (detailed in Chapter 2) was to develop a method to fluorescently label various apelin isoforms. Pyrene is a relatively inexpensive

fluorophore that is available conjugated to a variety of linker molecules. It can be used as a probe of microenvironmental polarity due its unique spectral properties (detailed in Sections 2.2.2-2.2.3), and therefore was a natural choice for examining peptide interaction with membrane mimetics. Pyrene-labelled peptides could then be used in many different types of experiments, probing both apelin-membrane interactions, as well as apelin-AR interactions. Methods developed for pyrene-apelin conjugation should also be readily generalizable to preparation of other apelin conjugates.

The second objective of this work (Chapter 3) was to use fluorescence spectroscopy to study the peptide-membrane interactions using three different membrane-mimetic surfactants: SDS, DPC, and 1-palmitoyl-2-hydroxy-*sn*-glycero-3-[phospho-*rac*-(1-glycerol)] (LPPG) (Figure 1.6). At concentrations above the critical micelle concentration (CMC), which is a value that is specific to the surfactant of interest, the monomeric, amphipathic molecules spontaneously assemble into spherical structures called micelles, with the hydrophilic surfactant headgroups forming the surface of the micelle, and the non-polar tails form the hydrophobic centre of the micelle (Figure 1.7). Surfactant micelles are the most frequently-used membrane-mimetics, particularly in NMR spectroscopy (26), so they are extremely relevant when it comes to comparison between experiments performed in the Rainey lab.

Aside from peptide-membrane interactions, pyrene-labelled apelin isoforms can also be used to examine peptide-receptor interactions. Specifically, pyrene acts a Förster resonance energy transfer (FRET) acceptor for tryptophan donors. The third and final objective of this work (Chapter 4) was, therefore, to test for the potential for interactions between the well-characterized AR55 segment of the AR and apelin ligands through the use of FRET.

Figure 1.1. Sequences of three naturally-occurring bioactive isoforms of apelin. Blue residues indicate the amino acids that are retained in all isoforms.

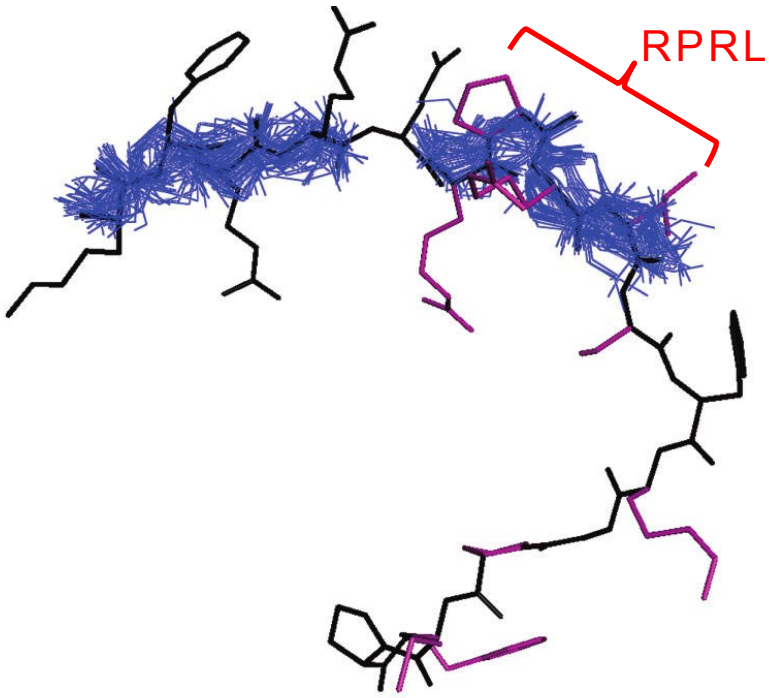

Figure 1.2. NMR ensemble of apelin-17 at 35 °C. The backbones of all 80 ensemble members are shown in blue for the two regions exhibiting increased structuring, superposed over the representative structure in black. Functionally critical residues are coloured in purple. RPRL motif denoted by red bracket. Reprinted with modifications with permission (Appendix i) from (16).

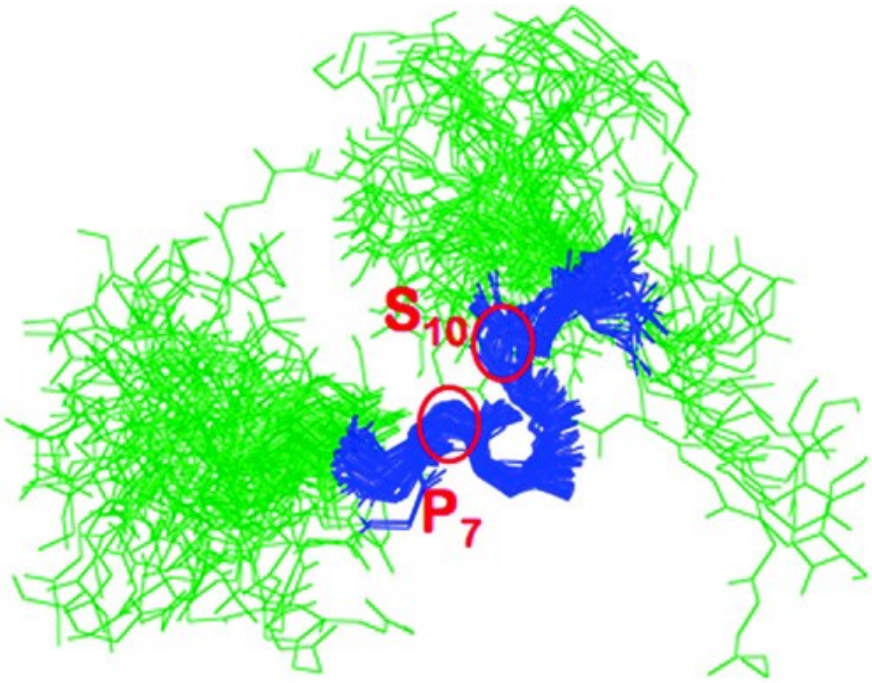

Figure 1.3. Structure of apelin-17 bound to an SDS micelle. Superposition of all 80 members of the final ensemble of structures from R6 to K12 (R6-K12 coloured blue, remainder green) with P7 and S10, initiation points of β-turns indicated. Reprinted with permission via the ACS Author Choice Usage Agreement, from (20).

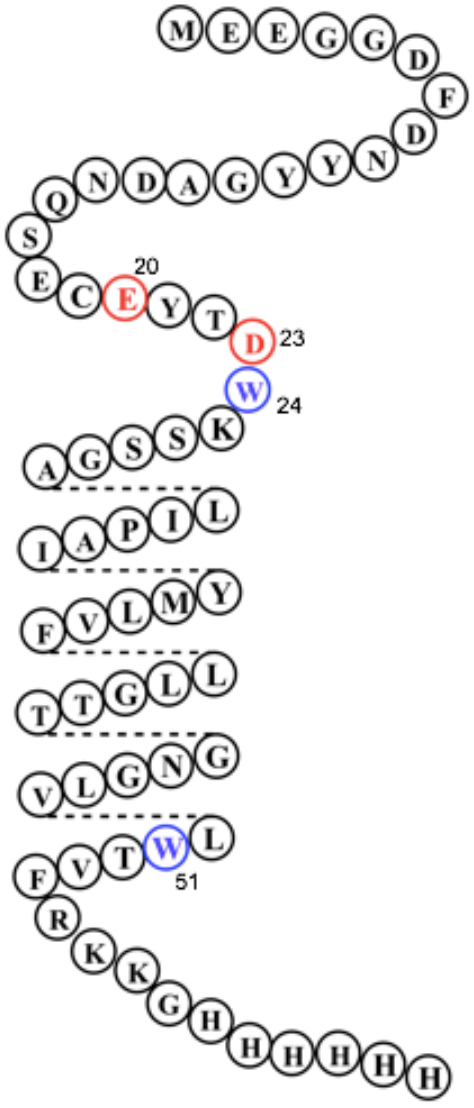

Figure 1.4. Snake-plot showing amino acid sequence of AR55 and its predicted topology. E20 and D23, key residues for binding according to mutagenesis (19), are highlighted in red, and the two native tryptophan residues, W24 and W51, are highlighted in blue. Modified from Aditya Pandey.

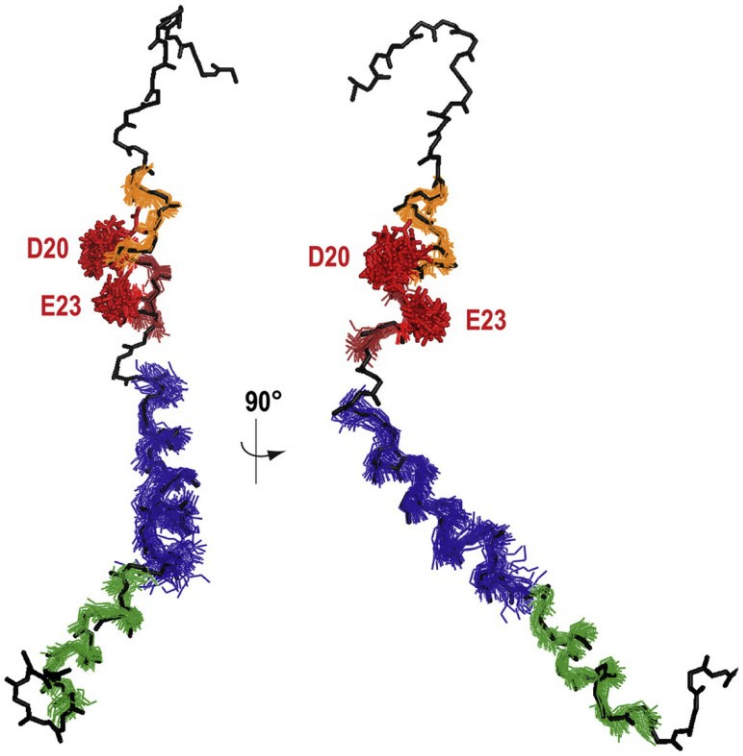

Figure 1.5. NMR structural ensemble (40-member) of AR55 in a DPC micelle containing solution. All four structurally converged regions within the NMR ensemble are superposed upon the lowest energy ensemble member (black), with D14-C19 in orange, E20-K25 in dark red, A29-N46 in blue, and G47-K57 in green. The E20 and D23 sidechains are shown for all 40 ensemble members with positions based on the backbone superposition of E20-K25. Reprinted with permission (Appendix ii) from (21).

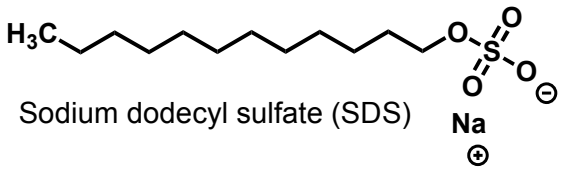

Sodium dodecyl sulfate (SDS)

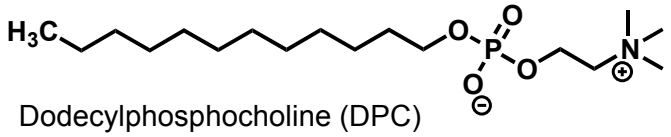

Dodecylphosphocholine (DPC)

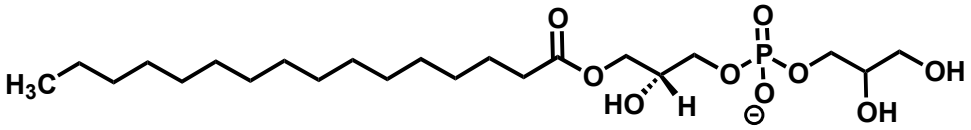

1-Palmitoyl-2-hydroxy-*sn*-glycero-3-[phospho-*rac*-(1-glycerol)]
(Lyso 1-palmitoyl phosphatidylglycerol - LPPG)

Figure 1.6. Chemical structures of surfactants used in this study: SDS, DPC, and LPPG.

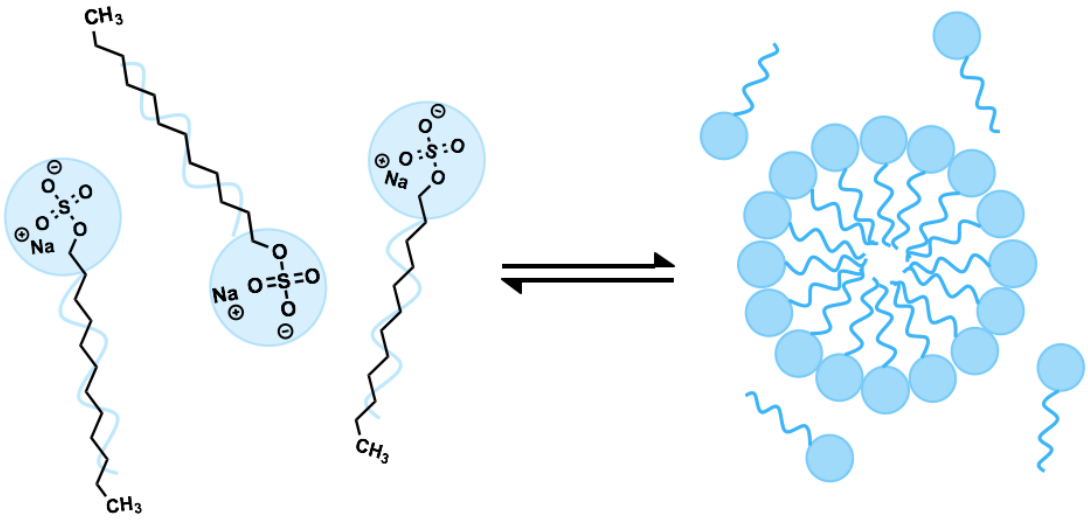

Figure 1.7. Schematic of SDS monomers (left) and an SDS micelle (right). Micelles assemble at concentrations above the critical micelle concentration (CMC). Round light blue circle represents polar headgroup; darker blue line represents non-polar tail.

Chapter 2: Fluorescent Labelling of Apelin Peptides

2.1. Introduction

Fluorescent labelling of peptides and proteins is a very useful tool in structural studies of protein complexes and interactions. Fluorescently labelled proteins have a vast array of experimental applications such as the use of fluorescence microscopy to examine protein localization within live cells or tissues. Polarity-sensitive probes, such as pyrene, can be used to examine the microenvironment surrounding the probe. Pairs of fluorescent tags can also be selected based upon appropriate spectral overlap in order to provide spatial information from energy transfer experiments. Examples of the latter two applications are further discussed in Chapters 3 and 4, respectively.

Green fluorescent protein (GFP) and other fluorescent proteins (FPs) have been widely used to study the organization of living systems since the early 1990s (27). However, FPs have several limitations. For example, the fluorophore component of FPs is generally buried in a β-barrel structure, protecting the fluorophore from the exterior environment and making precise detection of the surrounding microenvironment impossible (28). Most importantly, at 26.9 kDa (29), it is infeasible to fuse GFP to a small peptide such as apelin (1.5-4.2 kDa for the bioactive isoforms) without drastically changing the properties of the peptide. In order to examine localization of and intermolecular interactions on the nanometre scale involving small peptides, the use of fluorescent probes based upon small molecules is necessary.

Dyes derived from small molecules offer many advantages to FPs. In addition to being much more sensitive to environmental conditions such as polarity or pH, these dyes often offer the ability to selectively label specific positions within the protein of interest (POI).

Chemical dyes also generally have improved brightness and photostability over FPs (30). Furthermore, a vast selection of dyes are commercially available, often making it possible to select the exact spectral range and chemical conjugation method for a desired experiment. Targeting a specific position in the amino acid sequence of the POI can be made possible through the use of reactive linker molecules. In particular, cysteine and lysine possess side chain moieties that react with sulfhydryl, maleimide, or succinimidyl groups, and these reactions are among the most widely used for conjugating chemical dyes to proteins (30).

This chapter introduces a method for fluorescently labelling three different isoforms of apelin (Figure 1.1), making use of a reaction between an added N-terminal cysteine residue and a succinimide cross-linker. Apelin-12 and apelin-17 are readily synthesized using solid-phase peptide synthesis, and the N-terminal cysteine residue can be added during this process. Apelin-36 is longer and more difficult to synthesize using solid-phase synthesis; therefore, for the purposes of the experiments herein, it was expressed in and purified from *E. coli*. The N-terminal cysteine residue was added to a pre-existing open reading frame encoding apelin-36 using site-directed mutagenesis.

The N-terminus was chosen as the site for the fluorescent probe in hopes of affording the least disruption to biological activity, since the C-terminal phenylalanine residue of apelin-13 has been shown to be essential for activity (9) and many of the residues most susceptible to mutagenesis fall toward the apelin C-terminus (31). As such, conjugating a small molecule probe in close proximity to these residues could possibly hinder the activation mechanism. The thiol group of the N-terminal cysteine is regioselectively conjugated with a linker molecule, maleimide, which is in turn conjugated to a fluorescent molecule, pyrene (Figure 2.1). This maleimide-conjugated pyrene is called *N*-(1-

pyrenyl)maleimide (NPM). NPM has been used extensively to conjugate pyrene to cysteine residues for a wide range of applications, including examining the locations and spacing of cysteine residues in tubulin (32); determining the subunit orientation of translin (33); and, probing conformational changes in the helices of apolipophorin (34). The conjugation reaction is typically performed in either buffer (32, 35), or dimethylsulfoxide (36), with a 15-20 molar excess of NPM. This chapter introduces a new conjugation method performed in the aprotic solvent, dimethylformamide (DMF), which provides efficient labelling with only 2-5 M excess of NPM.

2.2. Materials and Methods

2.2.1. Materials

Acetonitrile and trifluoroacetic acid (TFA) were purchased from Fisher Scientific (Ottawa, ON). Primers were purchased from Bio Basic Canada (Markham, ON). BL21(DE3) strain *E. coli* cells were purchased from Lucigen (Middleton, WI). Ampicillin, isopropyl β-D-1-thiogalactopyranoside (IPTG) and reagents for lysogeny broth (LB) media were purchased from Fisher Scientific (Ottawa, ON). All other chemicals and solvents were obtained at reagent or high performance liquid chromatography (HPLC) grade from Sigma-Aldrich Canada (Oakville, ON), unless otherwise stated.

2.2.2. Peptide Synthesis and Purification

Solid-phase synthesis of the Cys-apelin-12 and -17 peptides was carried out by Nathan Weatherbee-Martin following standard protocols (16, 37). After lyophilization, each crude peptide product mixture was solubilized in water and analyzed using reversed-phase high performance liquid chromatography (RP-HPLC) on a Prostar HPLC equipped with a diode

array ultraviolet/visible (UV/Vis) absorbance detector (Varian Canada, Mississauga, ON) through monitoring of absorbance at 210 nm and 280 nm. For analytical purposes, a C_{18} matrix (5 μm particle, 4.6 mm x 250 mm Spirit Peptide column, AAPPTec, Louisville, KY) was employed with a water:acetonitrile (A:B; both containing 0.1% TFA) gradient with B progressing from 2 to 98% in 40 min at 0.8 mL/min flow rate. A preparative C_{18} matrix (5 μm particle, 20 mm x 250 mm Cosmosil column, Nacalai USA, San Diego, CA) employing the same gradient at a flow rate of 8 mL/min was used for purification purposes. Product mass was confirmed using positive mode electrospray ionization mass spectrometry (Dalhousie Mass Spectrometry Laboratory, Department of Chemistry, Halifax, NS).

2.2.3. Site-Directed Insertion Mutagenesis of Apelin-36

The pETHN vector was supplied from the laboratory of Dr. Paul Liu, and the apelin-36 gene from a template pET23 plasmid was subcloned into the pETHN vector immediately downstream of the 6xHis-SUMO gene by Nigel Chapman. 6xHis-SUMO-apelin-36 was mutated using the QuikChange mutagenesis kit (Stratagene, Wilmington, DE) according to the conditions in Table 2.1. A single cysteine residue was inserted immediately before L1 of apelin-36 (Figure 1.1). Forward and reverse primers had the sequences 5'-CAGATTGGTGGATGTCTGGTGCAGCC-3' and 5'-GGCTGCACCAGACATCCACCAATCTG-3', respectively. DNA sequencing (GENEWIZ, South Plainfield, NJ) was used to check for correct mutation with the amino acid sequence shown in Figure 2.2.

2.2.4. Expression and Purification of Cys-Apelin-36

To express 6xHis-SUMO-Cys-apelin-36, the BL21(DE3) strain of *E. coli* was transformed with the pETHN vector containing the 6xHis-SUMO-Cys-apelin-36 gene. The cells were grown for 16 h at 37 °C in a 250 mL Erlenmeyer flask containing 30 mL of LB medium with ampicillin (100 μg/mL). This culture was used to inoculate 2 L of LB medium with ampicillin (100 μg/mL), which was then grown to an optical density at 600 nm (OD_{600}) of 0.6. Expression was induced using IPTG (to a final concentration of 0.5 mmol/L). After induction, cells were grown for 3 h at 37 °C and harvested by centrifugation (6500g at 4 °C for 20 min).

The resulting cell pellet was resuspended in 30 mL lysis buffer (50 mmol/L NaH_2PO_4, 300 mmol/L NaCl, 10 mmol/L imidazole, titrated to pH 8.0 with NaOH) and the cells lysed using a French pressure cell press (American Instrument Company, Silver Springs, MD). The lysate was centrifuged at 15,000g for 30 min at 4 °C. 6xHis-SUMO-Cys-apelin-36 was purified from the supernatant using immobilized metal affinity chromatography with a Ni^{2+}-nitrilotriacetic acid (NTA) agarose column (Qiagen, Toronto, ON) that was pre-equilibrated with lysis buffer. The column was washed with 4 column volumes of wash buffer (50 mmol/L NaH_2PO_4, 300 mmol/L NaCl, 20 mmol/L imidazole, pH 8.0), and then the column-bound protein was collected upon the addition of elution buffer (50 mmol/L NaH_2PO_4, 300 mmol/L NaCl, 300 mmol/L imidazole, pH 8.0). Column flow-through, wash, and elution fractions were analyzed using SDS-PAGE (15% acrylamide), resolved at 180 V for 60 min, and visualized using Coomassie Blue stain. Elution fractions were combined, and the 6xHis-SUMO expression tag was cleaved from the protein using 200 μL recombinantly expressed SUMO protease (Addgene, Cambridge, MA; cloned and expressed by Nigel Chapman) and 1 mmol/L dithiothreitol (DTT), with incubation at room

temperature for 4 h. The cleavage product was lyophilized and resuspended in H_2O and Cys-apelin-36 was purified using RP-HPLC on a C_{18} semi-preparative matrix (5 μm particle, 10 mm x 250 mm Cosmosil column) with a water:acetonitrile (A:B; both containing 0.1% TFA) gradient with B progressing from 2 to 100% in 23 min with a non-linear gradient (20-42.5% B from 0-18 min, 42.5-100% B from 18-23 min) at 3.5 mL/min flow rate. Product mass was confirmed using positive mode electrospray ionization mass spectrometry (Dalhousie Mass Spectrometry Laboratory, Department of Chemistry, Halifax, NS)

2.2.1. Fluorophore Conjugation to Apelin Peptides

Purified Cys-apelin-12, -17 or -36 was dissolved in DMF (3 mg/mL) and incubated for 3 h at room temperature with 2-5 molar equivalents of NPM dissolved in 100 μL DMF. The reaction of Cys-apelin-36 included 5 mmol/L DTT. Reactions were monitored using RP-HPLC on a Prostar HPLC equipped with a diode array ultraviolet UV/Vis absorption detector (Varian Canada, Mississauga, ON) by monitoring absorbance at 210 nm and 340 nm using a C_{18} matrix (5 μm particle, 4.6 mm x 250 mm Spirit Peptide column) with a water:acetonitrile (A:B) gradient with B progressing from 2 to 100% in 25 min at 0.8 mL/min flow rate. Reaction mixture was purified on a preparative C_{18} matrix (5 μm particle, 20 mm x 250 mm Cosmosil column) using the same gradient with 8 mL/min flow rate. Product (Py-Cys-apelin-12 or -17) mass was confirmed using positive mode electrospray ionization mass spectrometry (Dalhousie Mass Spectrometry Laboratory, Department of Chemistry, Halifax, NS).

2.3. Results and Discussion

With the goal of conjugating a small molecule fluorescent probe at the N-terminus of three apelin isoforms, two apelin isoforms (apelin-12 and apelin-17 (Figure 1.1)) had been previously synthesized by solid-phase peptide synthesis with a cysteine residue added N-terminally to each natural human apelin sequence (Cys-apelin-12 and Cys-apelin-17). The synthetic cysteine-modified peptides were purified using RP-HPLC and their identities were confirmed using mass spectrometry. To obtain Cys-apelin-36 for conjugation, an existing pETHN vector containing the 6xHis-SUMO-apelin-36 gene was successfully mutated using site-directed insertional mutagenesis to incorporate a codon encoding a cysteine residue falling at the N-terminus of the apelin-36 sequence immediately C-terminal to the 6x-His-SUMO tag (6xHis-SUMO-Cys-apelin-36). Successful insertional mutagenesis was confirmed by DNA sequencing (Figure 2.2). Expression of the 6xHis-SUMO-Cys-apelin-36 protein was successfully induced with IPTG and initial Ni^{2+}-NTA purification was monitored using SDS-PAGE (Figure 2.3). Following enzymatic cleavage from the fusion protein, Cys-apelin-36 was purified by RP-HPLC (Figure 2.4), to a final yield of ~2 mg/L of LB medium.

The labelling reaction with the fluorescent probe NPM (Figure 2.1) was performed separately on each of the three purified, cysteine-modified apelin isoforms dissolved in DMF. DMF is a polar aprotic solvent that is typically used for solid-phase peptide synthesis (38). DMF was chosen because of its ability to dissolve the pyrene moiety (39), which consists of four fused benzene rings and has extremely limited solubility in aqueous solutions as well as alcohols or acetone. Highly charged apelin peptides are readily solubilized in DMF because of its polarity, but the lack of a labile proton prevents the solvent from interfering with the desired reaction.

Peptide bonds absorb UV light in the 180-230 nm range. The aromatic amino acid side chains also absorb in this region, in addition to the longer wavelength 240-300 nm region (40). Pyrene absorbs strongly from 300-350 nm, with the absorbance maximum at 340 nm (41). The fact that pyrene absorbs at longer wavelengths than peptides or proteins means that its absorption can be used to monitor the progress of the reaction using an RP-HPLC equipped with a UV/Vis absorption detector that allows monitoring of at least two wavelengths. In Cys-apelin modification (Figure 2.1), monitoring of the eluent at both 210 nm and 340 nm allows straightforward identification of both the peptide and pyrene starting materials peaks on the chromatogram, since the unreacted protein will not absorb at 340 nm. As the reaction progresses, the appearance of a new peak showing absorbance at 340 nm is indicative of product formation.

It was found that the NPM conjugation reaction proceeded efficiently at room temperature at as little as a 2:1 molar ratio of NPM to peptide. Monitoring by RP-HPLC at increasing time points throughout the reaction revealed that the reaction proceeded quickly, with the starting material nearly completely reacted after just one hour (Figure 2.5). When monitoring the reaction of Cys-apelin-36 with NPM, it was noted after three hours that a product peak had not yet appeared. However, with the addition of 5 mmol/L DTT the reaction progressed similarly rapidly as with the other apelin isoforms. This indicates that the starting material, Cys-apelin-36 was more dimeric in nature than Cys-apelin-12 or -17, and the disulphide bonds prevented the reaction from proceeding between the thiol group of the cysteine and the maleimide linker molecule.

The putative product peaks exhibiting both protein and pyrene absorption from the reaction mixture for each isoform were collected, lyophilized, and analyzed using mass spectrometry. Peaks exhibiting the m/z ratio for each singly NPM-labelled Cys-apelin

isoform species were predominant (Figure 2.6-2.7, Tables 2.2-2.3). Thus, the addition of a cysteine residue at the N-terminus of three different isoforms of apelin allows for efficient and specific labelling with a fluorescent probe.

This technique can be modified to suit the particular experiment of interest. Because of the versatility of DMF as a solvent, the relatively low stoichiometric excess required vs. literature protocols, and the variety of fluorescent probes with maleimide linkers that are commercially available, it is likely that this method could be used for any number of different fluorescent dyes, making it possible to conjugate a dye with specific spectral properties tailored to the desired experiment. It would also be feasible to synthesize or mutate apelin isoforms with a cysteine residue in different positions in the sequence to probe other areas of the peptide such as in the RPRL motif or at the C-terminus, areas of apelin previously shown in work from the Rainey lab to be critical for function (16).

In order to assess the bioactivity of the pyrene-labelled peptides, Nigel Chapman performed a phosphorylated extracellular signal-regulated kinase (pERK) dose-response assay in apelin receptor-transfected human embryonic kidney (HEK-293) cells. After transfection, HEK-293 cells were stimulated with a range of Py-Cys-apelin-12 concentrations (10^{-10} M – 10^{-5} M) and compared to a non-stimulated sample. Immediately after stimulation, cells were harvested and lysed, and lysates were examined using SDS-PAGE and western blot analysis. Quantities of pERK were analyzed for each sample using ERK as a loading control (Figure 2.8). It was found that Py-Cys-apelin-12 had a shifted dose-response curve compared to that of wild-type (WT) apelin-13 (data from Nigel Chapman). The half-maximal effective concentration (EC_{50}) was found to be ~80 nmol/L for Py-Cys-apelin-12, whereas WT apelin-13 was found to have an EC_{50} of ~0.2 nmol/L. This corresponds to a significant decrease in the potency of the pyrene-labelled species;

however, it was found that the maximal effect (E_{max}) for Py-Cys-apelin-12 was ~3.2, comparable to that for WT apelin-13 at ~2.8. While the mechanism by which the decrease in potency remains unclear, the pyrene-labelled peptide still elicited a full response from the AR. This result was considered adequate to pursue further experiments with Py-Cys-apelin-12 in solution with membrane mimetics.

2.4. Summary

An efficient method has been developed for the site-specific fluorescent labelling of three isoforms of apelin. The method has been shown to be effective for synthetic forms of apelin-12 and -17 and for recombinantly expressed apelin-36. The only requirements are that there be a cysteine residue in the sequence in the desired location, and that the fluorophore of interest is available with a maleimide linker molecule. This technique could be extremely useful in future experiments to probe other areas of the apelin sequence, or to test the use of other fluorophores with different spectral properties.

Table 2.1. The reaction composition and thermocycling conditions used for mutagenesis of apelin-36.

Reaction composition	
Buffer type and amount	1x Phusion HF reaction buffer, 10 μL
Template DNA (ng)	50
[Primers] (μmol/L)	0.2
dNTPs (μL)	1
Polymerase type and amount	Phusion, 1 U
Cycling conditions	
Initial denaturation	98 °C, 30 s
Number of cycles	25
Melting step	98 °C, 30 s
Annealing step	66 °C, 60 s
Extension step	72 °C, 3.5 min
Final extension	N/A

Table 2.2. Mass spectrometry deconvolution corresponding to Figure 2.6, Py-Cys-apelin-12. Expected monoisotopic mass = 1821.86. Discrepancy due to the fact that Py-Cys-apelin-12 will statistically incorporate 1 ^{13}C atom per molecule.

m/z	Charge	$M^{+\bullet}$
608.6	3+	1822.78
456.7	4+	1822.77
365.6	5+	1822.96

Table 2.3. Mass spectrometry deconvolution corresponding to Figure 2.7, Py-Cys-apelin-17. Expected monoisotopic mass = 2537.28. Discrepancy due to the fact that Py-Cys-apelin-17 will statistically incorporate 1 ^{13}C atom per molecule.

m/z	Charge	$M^{+\bullet}$
847.1	3+	2538.28
635.6	4+	2538.37
508.7	5+	2538.46

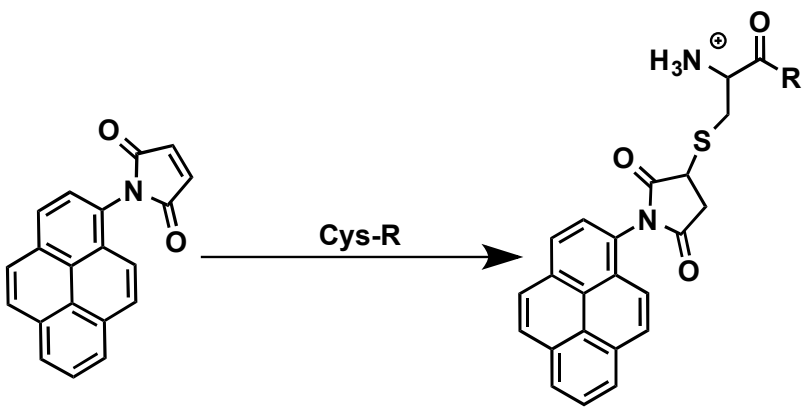

Figure 2.1. Chemical reaction between *N*-(1-pyrenyl)maleimide (NPM) and thiol group of cysteine side chain.

HHHHHHGSDS EVNQEAKPEV KPEVKPETHI NLKVSDGSSE
IFFKIKKTTP LRRLMEAFAK RQGKGMDSLR FLYDGIRIQA
DQTPEDLDME DNDIIEAHRE QIGGCLVQRP GSRNGPGPWQ
GGRRKFRRQR PRLSHKGPMP F

Figure 2.2. Amino acid sequence of 6xHis-SUMO-Cys-Apelin-36. 6xHis tag shown in green, SUMO sequence shown in purple, cysteine insertion mutation shown in red, apelin-36 sequence shown in blue.

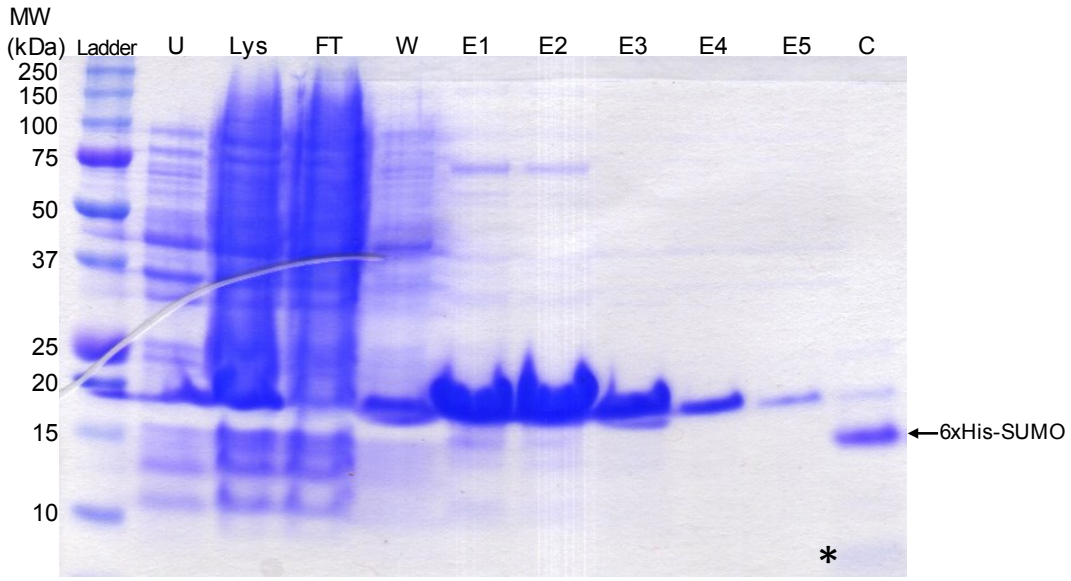

Figure 2.3. A 15% acrylamide SDS-PAGE after electrophoresis and Coommassie Blue staining showing initial expression and purification of Cys-apelin-36. The protein ladder is shown on the left. U, uninduced; Lys, whole-cell lysate; FT, Ni^{2+}-NTA column purification flow-through fraction; W, wash fraction; E1-E5, elution fractions 1-5; C, after enzymatic cleavage. Arrow points to band corresponding to the 6xHis-SUMO cleavage product, Cys-apelin-36 is denoted by *.

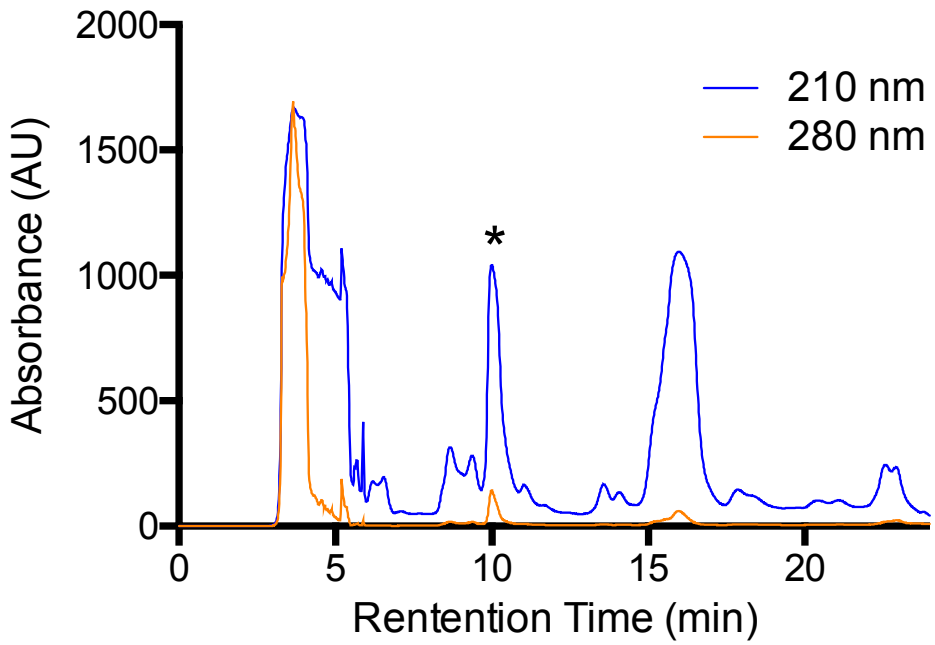

Figure 2.4. RP-HPLC chromatogram showing purification of Cys-apelin-36 monitored at 210 nm (blue) and 280 nm (orange). Purification was carried out on a C18 semi-preparative matrix (5 μm particle, 10 mm x 250 mm Cosmosil column) with a water:acetonitrile (A:B; both containing 0.1% TFA) gradient with B progressing from 2 to 100% in 23 min with a non-linear gradient (20-42.5% B from 0-18 min, 42.5-100% B from 18-23 min) at 3.5 mL/min flow rate. Large peak at ~16 minutes corresponds to cleaved 6xHis-SUMO fragment. Cys-apelin-36 peak is denoted by *.

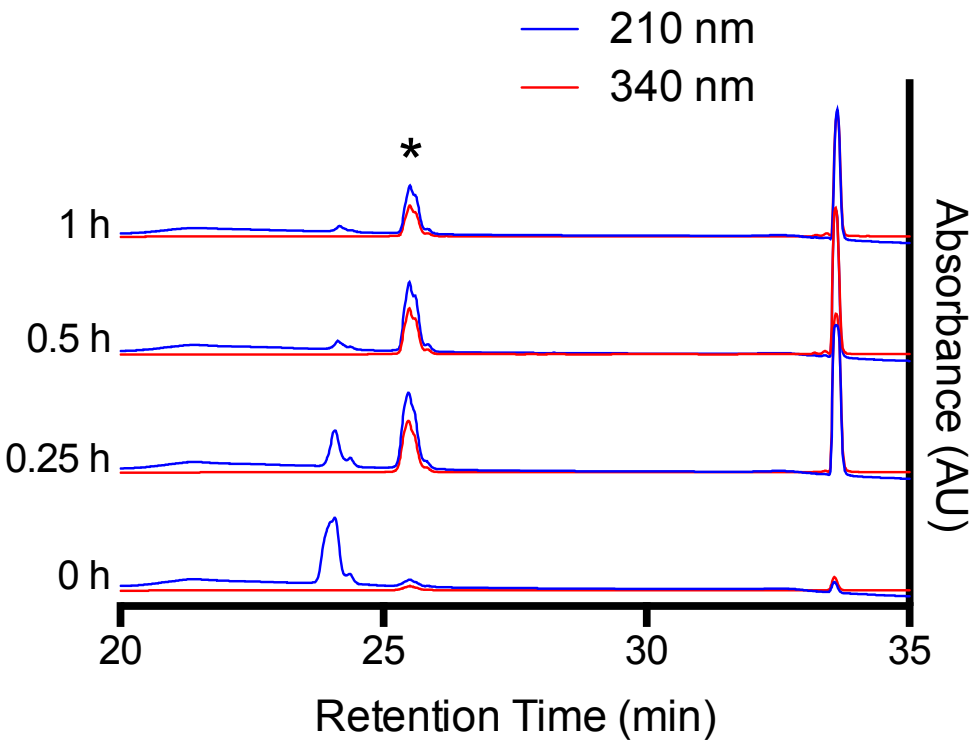

Figure 2.5. RP-HPLC monitoring of reaction between NPM and Cys-apelin-12, monitored at 210 nm (blue) and 340 nm (red). Analytical monitoring was performed using a C18 matrix (5 μm particle, 4.6 mm x 250 mm Spirit Peptide column) with a water:acetonitrile (A:B) gradient with B progressing from 2 to 100% in 25 min at 0.8 mL/min flow rate. Left vertical axis indicates time in hours after the start of the reaction. Peak at ~24 min corresponds to Cys-apelin-12, peak at ~26 min corresponds to the reaction product Py-Cys-apelin-12, denoted by *. The peak at ~34 min corresponds to unreacted NPM.

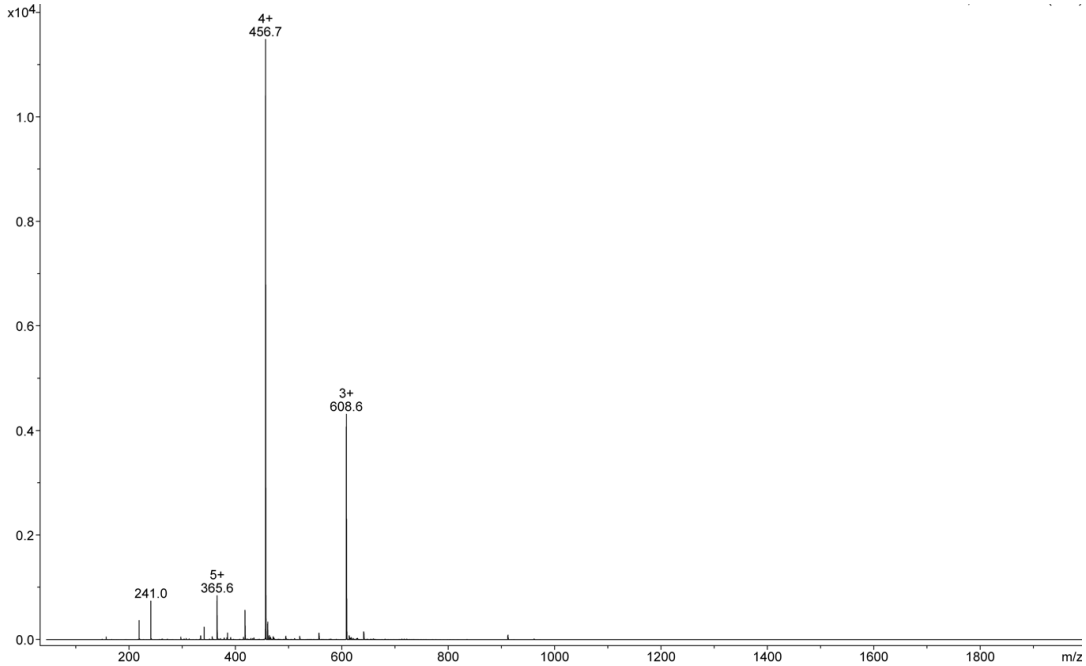

Figure 2.6. Positive mode electrospray ionization mass spectrometry analysis of Py-Cys-apelin-12. Molecular ion mass ($M^{+\bullet}$) is 1823 amu, expected mass is 1822 amu. Deconvolution analysis found in Table 2.2.

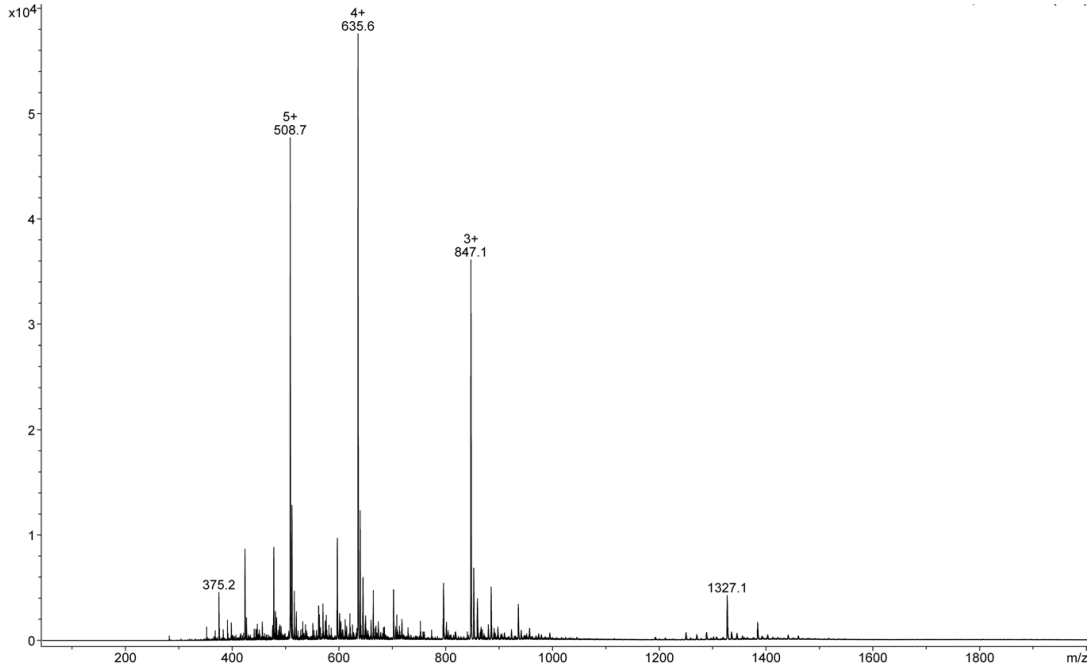

Figure 2.7. Positive mode electrospray ionization mass spectrometry analysis of Py-Cys-apelin-17. Molecular ion mass ($M^{+\bullet}$) is 2538 amu, expected mass is 2537 amu. Deconvolution analysis found in Table 2.3.

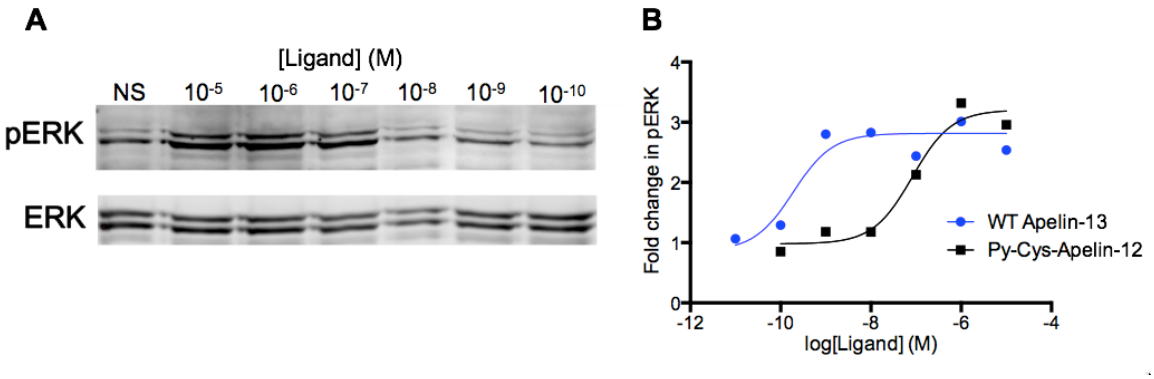

Figure 2.8. Phosphorylated extracellular signal-regulated kinase (pERK) assay in apelin receptor-transfected HEK-293 cells. ERK serves as a loading control. NS, no stimulation; n=1. A) Western blot analysis. B) Graphical analysis. Data from Nigel Chapman.

Chapter 3: Examining Peptide-Micelle Interactions Using Fluorescence Spectroscopy

3.1. Introduction

As introduced in Section 1.2, it has previously been shown by the Rainey lab that apelin interacts with membrane-mimetic surfactant micelles (20). Langelaan and Rainey found that the CD spectra for both apelin-12 and apelin-17 in buffer indicate that both isoforms are random coil in nature (16); however, in the presence of anionic SDS and LPPG micelles, both isoforms exhibit far-UV CD spectra with a convoluted α-helical band pattern. These findings were confirmed by nuclear magnetic resonance (NMR) spectroscopy for apelin-17. Diffusion coefficients calculated from NMR spectroscopy data indicate that apelin-17 binds favourably with SDS and LPPG, and experiences weak, transient binding to zwitterionic DPC micelles. The calculated structure for apelin-17 showed that the key to this interaction is a converged structure from R6 to K12 (Figure 1.1, 1.3), as well as structuring of M15 to M17, which does not directly interact with the micelle surface (20). It was concluded that these findings indicate that apelin likely fits with the membrane catalysis theory put forth by Sargent and Schwyzer in 1986 (25). This chapter discusses a method by which this interaction can be evaluated using fluorescence spectroscopy on pyrene-labelled apelin peptides.

3.1.1. Fluorescence Spectroscopy

Fluorescence spectroscopy is a technique that exploits the inherent photoluminescent properties of molecular groups known as fluorophores. Photoluminescence is the emission of light from an excited state, and this emission can be divided into two categories: fluorescence and phosphorescence. The defining difference between the two categories is

that phosphorescence occurs from an excited triplet state and fluorescence occurs from an excited singlet state (42). This chapter will focus on fluorescent emission.

Fluorophores, also called fluorescent probes or dyes, are typically aromatic compounds, and can either be intrinsic (a natural component of the system) or extrinsic (added to the system). Examples of intrinsic fluorophores are the aromatic amino acids: tryptophan, tyrosine and phenylalanine. Extrinsic fluorophores are molecules that have been labelled with a fluorophore that is not naturally occurring (43), for example pyrene, which is discussed in this chapter. Fluorophores can be used to examine many different aspects of a biological system. Examples include detecting binding between two proteins like a GPCR and a G-protein in living cells (44), examining protein localization in living cells (45), or providing insight into protein structure and conformation *in vitro* (46), just to name a few.

Both intrinsic and extrinsic fluorophores emit light following the same mechanism, which is most often described by a schematic known as a Jablonski diagram (Figure 3.1), first used by Professor Alexander Jablonski in 1935 (47). The Jablonski diagram shows how after absorption of UV or visible light, the fluorophore promotes an electron to an excited state, usually a higher vibrational level of the S_1 or S_2 singlet states. Typically, the electron then relaxes to the lowest energy vibrational S_1 state. Vibrational relaxation takes place within a given singlet state, while relaxation from higher to lower (e.g., S_2 to S_1) singlet states occur through a process called internal conversion. Both vibrational relaxation and internal conversion happen very rapidly, generally before emission (42). From the lowest vibrational S_1 state level, the electron then relaxes to the S_0 ground state. This may occur radiatively, leading to emission of a photon, or nonradiatively. Relative rates of these processes differ from fluorophore to fluorophore, with those having a higher rate of radiative vs. non-radiative emission having a higher quantum yield. The quantum yield is

defined as the ratio of the number of photons emitted compared to the number of photons absorbed (42). Radiative relaxation results in the emission of a photon that is lower in energy, and thus higher in wavelength than the excitation photon. The difference between the excitation wavelength and the emission wavelength was first noted by Sir George Gabriel Stokes in 1852 (48), and is referred to as the Stokes shift. Because of the initial, rapid relaxation to the lowest vibrational S_1 state after excitation, the emission of most fluorophores is not affected by the excitation wavelength. However, because electrons typically relax to a vibrational energy level above the lowest vibrational level of the S_0 state, an emission spectrum can show multiple bands resulting from photons of varying energy due to relaxation to multiple vibrational levels.

The instrument used to examine fluorescence is called a spectrofluorometer, often shortened to fluorometer. A basic spectrofluorometer comprises three major components: a light source, a monochromator, and a detector (Figure 3.2). Light is emitted from the light source, typically a xenon or mercury lamp, and travels through a monochromator that selects the desired wavelength. Most monochromators use a diffraction grating to separate the wavelengths of light. The selected wavelength is then passed through a slit, the width of which can be adjusted to let through the desired range of wavelengths. Slit widths for fluorescence spectroscopy experiments are generally 2 nm to 10 nm. The light is then passed through the sample compartment, where the fluorophores present in the sample are allowed to undergo absorption. The subsequent emission process is usually detected at a 90° angle, and the emission light is passed through a second monochromator, where the desired emission wavelength is selected. From there, the emission photons pass through to the detector, which is usually a photomultiplier tube (PMT). PMTs work by multiplying the signal from each photon so that the final signal is many, many times greater than the

initial emission signal. A photon that enters the PMT hits a photocathode, which causes an electron to be ejected. The ejected electron is then accelerated toward the first dynode, where upon impact, another 5-20 electrons are ejected (49). These electrons then travel toward the second dynode, where they each cause the ejection of more electrons, and the process continues down the chain of dynodes until the electrons hit the anode, where they are converted into an emission signal. The emission intensities for each wavelength are pieced together to give an emission spectrum.

3.1.2. Pyrene as a Polarity-Sensitive Probe

Pyrene is a small fluorescent probe that is often used in biophysical studies because of its unique fluorescent properties. Pyrene exhibits five characteristic emission bands, denoted as bands I-V, that correspond to the five vibronic transitions. These bands are collectively referred to as the monomer bands. The monomer band spectrum can be used to examine the nature of the environment surrounding the pyrene as the intensities of bands I and III are highly sensitive to polarity (50). The first excited state of pyrene is generally forbidden or weakly allowed, compared to the strongly allowed second excited state. However, in the presence of polar solvent or other closely associated molecules, the first excited state is stabilized by dipole-dipole interactions, which enhances the vibronic coupling between S_1 and S_2, resulting in an increase in the ratio of the intensity of band I compared to band III (51-53). This ratio can be used to evaluate the polarity of the environment surrounding the pyrene, and is known as the *Py* scale, first defined by Dong and Winnik in 1982 (54). The scale ranges from 0.58 for pyrene in hexane to 1.95 for pyrene in dimethylsufoxide (55). The *Py* scale has previously been used by Tamamizu-Kato *et al.* to probe protein binding to membrane mimetics (56). The theory is that an

increase in *Py* value upon addition of membrane-mimetic micelles indicates that the pyrene moiety is located in the highly polar, hydrophilic surface of the micelles. A decrease in the *Py* value indicates that the pyrene group is located in the non-polar, hydrophobic centre of the micelles. In order to measure an interaction with surfactant micelles, the surfactant concentrations must be above the critical micelle concentrations (CMC). The CMC is the concentration above which the particular surfactant spontaneously forms micelles in solution. Having a concentration well above the CMC ensures that the concentration of surfactant remaining as a monomer is negligible compared to the concentration of micellar surfactant. A high micelle to peptide ratio also limits pyrene excimer formation, further discussed in the following section.

3.1.3. Pyrene Excimers

The second unique spectral property of pyrene is its ability to form excited dimers, or "excimers", first defined by Stevens and Hutton in 1960 (57). An excimer is a dimer that associates in the excited electronic state, but dissociates in the ground state (58). Excimer formation follows the simplified mechanism:

$$M + hv = M^* \tag{3.1}$$

$$M + M^* = E^* \tag{3.2}$$

where M is a monomer in the ground state that absorbs a photon, promoting it to a singlet excited state, M^*. Under normal circumstances, M^* would relax back to the ground state by emitting a photon in the process known as fluorescence. However, pyrene has an exceptionally long excited state lifetime of 40-90 ns (59), so the excited state monomer is able to interact with other ground state monomers if they are within ~10 Å, giving rise to

an excimer, E^*. Excimer formation is characterized by a broad, unstructured band that is significantly red-shifted compared to the monomer emission bands (~410-460 nm).

The appearance of the excimer band can be used to provide structural information about pyrene-labelled proteins. Sahoo *et al.* used excimer emission from double pyrene-labelled apoliophorin III to determine a conformational switch from a helical bundle to an extended helical organization upon addition of lipids (60). Excimer emission has also been used extensively to examine CMC, aggregation number, and other properties of surfactant micelles (61-63). However, for the present studies, excimer emission, or lack thereof, was used as a control to ensure that the micelle to peptide ratio was great enough that protein-protein interaction was not affecting the observations.

3.2. Materials and Methods

3.2.1. Materials

DPC was purchased from Anatrace (Maumee, OH). LPPG was purchased from Avanti Polar Lipids (Alabaster, AL). SDS was purchased from Fisher Scientific (Ottawa, ON). All other materials were purchased from Sigma-Aldrich Canada (Oakville, ON), unless otherwise stated.

3.2.2. Peptide-Micelle Interaction Fluorescence Spectroscopy Experiments

Lyophilized labelled peptide concentrations were obtained by UV/Vis absorbance spectrophotometry using a molar extinction coefficient (ε) of 40,000 M^{-1} cm^{-1} at 338 nm for pyrene (64). Methanol solutions were then lyophilized, and peptide stock solutions were made at concentrations of 150 μmol/L. Surfactant stock solutions of SDS, DPC and LPPG were made at concentrations of 160 mmol/L each. Final samples were diluted to 1 μmol/L

peptide and 100 mmol/L surfactant in 20 mmol/L sodium phosphate buffer with 60 mmol/L NaCl at pH 7.0, unless otherwise stated.

All steady-state fluorescence spectroscopy experiments were carried out on a Horiba Photon Technology International (Horiba PTI, London, ON) QuantaMaster-4CW spectrofluorometer controlled using Felix32 software (PTI). Samples were analyzed in a 3 mm x 3 mm quartz microcuvette (Hellma Analytics, Markham, ON) using 150 μL volumes at 37 °C. Both excitation and emission monochromators were set at 4 nm slit widths. The excitation wavelength (λ) for all pyrene-labelled samples was 340 nm and emission spectra were recorded from 350 nm – 550 nm with an integration time of 0.25 nm/s. Each experiment was repeated three times using fresh samples and spectra were averaged and blank subtracted. Spectra were analyzed using GraphPad Prism 6 (GraphPad Software, San Diego, CA).

3.2.3. Control Experiments

NPM was conjugated to mercaptoethanol following the method described in Section 2.2.1. Briefly, mercaptoethanol was dissolved DMF and incubated for 3 h at room temperature with 2-5 molar equivalents of NPM dissolved in 100 μL DMF. The reaction was monitored using RP-HPLC on a Prostar HPLC equipped with a diode array UV/Vis absorbance detector through monitoring of absorbance at 210 nm and 340 nm. For analytical purposes, a C_{18} matrix (5 μm particle, 4.6 mm x 250 mm Spirit Peptide column) was employed with a water:acetonitrile (A:B; both containing 0.1% TFA) gradient with B progressing from 2 to 100% in 25 min at 0.8 mL/min flow rate. A preparative C_{18} matrix (5 μm particle, 20 mm x 250 mm Cosmosil column) employing the same gradient at a flow rate of 8 mL/min was used for purification purposes. Lyophilized product (Py-

mercaptoethanol) was dissolved in methanol and concentration was obtained by UV/Vis spectrophotometry using ε=40,000 M^{-1} cm^{-1} at 338 nm for pyrene (64). The methanol solution was lyophilized and a stock solution was made at a concentration of 150 μmol/L in ethanol. A separate stock solution of pyrene was made at a concentration of 150 μmol/L in ethanol.

All control experiments were performed exactly as described in Section 3.2.2, except using the ethanol pyrene and Py-mercaptoethanol stocks instead of Py-Cys-apelin.

3.2.4. Calculation of *Py* Values

Py values were calculated for each spectrum by selecting the local maximum around 375 nm – 385 nm as band I. Band III for all spectra was selected as 10 nm red shifted from band I. After background signal subtraction, the *Py* value was calculated as follows:

$$Py = \frac{F_I}{F_{III}} \tag{3.3}$$

where F_I is the emission intensity of band I and F_{III} is the emission intensity of band III. Ratios were calculated for each experimental replicate and are reported as an average with the standard error of the mean (SEM). P values were calculated from the SEM using a statistics calculator on http://www.graphpad.com/quickcalcs/ by an unpaired t test. P values are denoted as follows: $p>0.05$, not significant (ns); $p\leq 0.05$, *; $p\leq 0.01$, **; $p\leq 0.001$, ***; $p\leq 0.0001$, ****.

3.3. Results and Discussion

Fluorescence emission spectra were acquired for all three pyrene-labelled isoforms of apelin (Py-Cys-apelin-12, -17, and -36) and for pyrene and the NPM-mercaptoethanol conjugate (Py-mercaptoethanol) in the absence of surfactant and in the presence of SDS,

DPC and LPPG surfactant micelles (Figure 3.3-3.4). Unless otherwise stated, fluorescence experiments were repeated three times using fresh samples for each repeat, and spectra were averaged. Pyrene-labelled peptide samples were excited at the pyrene absorption maximum (340 nm) and emission spectra were collected from 350 nm to 550 nm. The same general trend was observed for each sample type across all three peptides, while some differences in behaviour were observed for the controls relative to the conjugated peptide samples.

First, emission intensity was found to increase with the addition of each of the three surfactants relative to buffer. This was true for all three isoforms of pyrene-labelled apelin, as well as the two control samples. An increase in emission intensity, or quantum yield, across the entire observed spectrum is likely due to a decrease in non-radiative decay processes (65). It is possible that binding of apelin to the micelle would reduce collisional quenching of the fluorophore, leading to an overall increase in observed emission intensity (66).

Second, a slight red shift of the emission spectrum was observed as a function of increasing apelin isoform length, where Py-Cys-apelin-12 showed a maximum band at 382 nm, Py-Cys-apelin-17 had a maximum at 385 nm, and Py-Cys-apelin-36 at 386 nm (Figure 3.3). Emission spectra of all three apelin isoforms were significantly red-shifted compared to the two control spectra. Pyrene showed a maximum band at 374 nm and Py-mercaptoethanol showed a maximum band at 376 nm (Figure 3.4). The slight red shift observed for Py-mercaptoethanol compared to pyrene could be due to the addition of the electron-donating maleimide group at the 1-position on pyrene, which slightly extends the electron delocalization, lowering the energy of the lowest unoccupied molecular orbital (LUMO) and resulting in a red-shifted emission wavelength (67). The increased shift

observed with Py-Cys-apelin peptides could perhaps be due to further extension of the electron delocalization throughout the protein backbone.

Py values were calculated for each spectrum by selecting the local maximum around 375 nm – 385 nm as band I. Band III is located in a trough of the spectrum for many of the samples, so for all spectra it was selected as 10 nm red shifted from band I based on the spectrum for pyrene which was in line with literature values (41). The *Py* values were calculated as a ratio of the emission intensity of band I/band III. A *Py* value of less than 1 indicates a highly hydrophobic environment surrounding the pyrene moiety, with increasing *Py* values suggesting increasing hydrophilicity (41). It was found that the *Py* value for Py-Cys-apelin in sodium phosphate buffer in the absence of surfactant was ~1.4 for all three isoforms (Table 3.1, Figure 3.5-3.7). The pyrene control sample had a similar *Py* value of 1.49 in the absence of surfactant (Figure 3.8), whereas the Py-mercaptoethanol control sample had a value of 2.34 (Figure 3.9); however, all data for Py-mercaptoethanol were found to be inconsistent with the trends observed for every other sample. This anomaly is further discussed later in the chapter.

Each surfactant was added to a concentration of 100 mmol/L, which is considerably higher than the CMCs of ~4 mmol/L (68), ~1.1 mmol/L, and ~0.02 mmol/L (69) for SDS, DPC, and LPPG, respectively. It was found that with the addition of SDS surfactant micelles, the *Py* value for each Py-Cys-apelin-12 and -36 increased to ~1.6 while for Py-Cys-apelin-17 it increased to ~1.8. This significant increase in observed *Py* value for all three isoforms implies that the pyrene group is located in the highly charged area on the surface of the surfactant micelles. The *Py* values for all three isoforms in the presence of zwitterionic DPC micelles were between 1.75 and 1.8. In the presence of anionic LPPG micelles, Py-Cys-apelin-12 and -36 had similar *Py* values around 1.75, whereas Py-Cys-

apelin-17 had a higher value of 1.85. The general trend for all three isoforms of pyrene-labelled apelin is a significant increase in *Py* value with the addition of anionic or zwitterionic surfactant micelles. This trend does not appear to depend on the concentration of Py-Cys-apelin, since increasing the concentration up to 10 μmol/L, does not significantly change the normalized spectra (Figure 3.10).

In previous studies, it was shown that apelin-12 and -17 bind favourably to anionic micelles of SDS and LPPG, and show a weaker, more transient interaction with zwitterionic DPC micelles (20). In the current study, it is not possible to distinguish the type of interaction taking place between anionic vs. zwitterionic micelles. In fact, the *Py* values from the DPC samples for both Py-Cys-apelin-12 and -36 were slightly greater than those of the anionic micelle samples. This could be explained by the fact that the *Py* value is a function of the interaction between pyrene and the surrounding environment, which is influenced by several factors including hydrogen bonding and dipole moment of the solute and solvent (41), and it has been suggested that the *Py* value is most strongly influenced by the dipole moment of the surrounding molecules (51). The DPC headgroup (Figure 1.6) has a dipole moment of ~15 D (70) whereas the SDS headgroup has a much smaller dipole moment of ~4.7 D (71). The dipole moment for the LPPG headgroup is not available in the literature, however a similar molecule, [(1*R*)-1-[[[(2*S*)-2,3-dihydroxypropoxy]-hydroxy-phosphoryl]oxymethyl]-2-hexadecanoyloxy-ethyl] (*z*)-octadec-11-enoate (which has the same headgroup as LPPG but with two alkyl chains instead of one (Figure 3.11)) has a dipole moment of ~5.3 D (72), comparable to SDS. Therefore, it is possible that because the DPC headgroup has a much larger dipole moment than SDS or LPPG, even if the binding interaction between the peptide and micelle is weaker, the dipole-dipole interaction is stronger resulting in a greater *Py* value.

Notably, there is no evidence of pyrene excimers for any of the samples at the experimental concentrations. In earlier experiments with lower concentrations of SDS below the CMC (less than 4 mmol/L), and higher concentrations of Py-Cys-apelin-12 (~10 μmol/L), a broad excimer band appeared above 450 nm (Figure 3.12), indicating that the pyrene groups were in close enough proximity (less than 10 Å) to form an excimer. In all of the present experiments, the absence of this excimer band indicates that the micelle to peptide ratio is great enough that there is less than one peptide per micelle, and that the amphipathic Py-Cys-apelin molecules do not form separate micelles in solution.

Py values for the pyrene control were found to have the opposite trend (Figure 3.8); upon addition of SDS, DPC, or LPPG micelles, they decreased to ~1 (Table 3.1), which indicates that the pyrene is likely being incorporated into the hydrophobic centre of each type of surfactant micelles. This difference in behaviour for pyrene alone vs. the pyrene conjugated apelin peptides demonstrates that conjugation of pyrene to the peptide does not significantly alter the behaviour of the peptide in the surfactant solution, as there is no evidence to suggest that the peptides are incorporated into the centres of the micelles.

Py-mercaptoethanol control samples showed an interesting, however puzzling, trend (Figure 3.9). *Py* values for all four samples including the buffer sample as well as each of the three surfactants were above 2. In the absence of surfactant, the value was 2.34. There was no significant change with the addition of zwitterionic DPC micelles. With the addition of anionic SDS or LPPG micelles, the *Py* value increased slightly to 2.55 and 2.44, respectively. This slight increase could indicate a somewhat more favourable interaction with anionic surfactant micelles as compared to zwitterionic micelles; however, the most important information obtained from this control experiment is that, unlike pyrene, there is no evidence to suggest that NPM is incorporated into the hydrophobic centres of the

surfactant micelles. It is possible that the maleimide moiety conjugated to mercaptoethanol provides enough polarity to prevent the highly hydrophobic pyrene group from solubilizing inside the micelles. However, it still remains a question as to why the *Py* values for all Py-mercaptoethanol samples were so much greater than any of the apelin samples or the pyrene control. Perhaps the presence of the hydroxyl group on mercaptoethanol in such close proximity to the pyrene moiety effectively enhances the polarity of the environment enough to perturb the *Py* values; however, more experiments with different groups conjugated to the NPM are required to provide a more conclusive answer. Although the exact cause for this anomaly remains unclear, the minimal differences across all four Py-mercaptoethanol samples imply that the significant changes that are observed with Py-Cys-apelin experiments are due to interactions between apelin and the surfactant micelles, and the behaviour of the peptides is not significantly altered due to the NPM group.

This chapter has demonstrated a valuable protocol for qualitatively assessing an interaction between a peptide and surfactant micelle. With the exception of the work done by Tamamizu-Kato *et al.* on α-synuclein (56), there are very few published examples of the use of the *Py* scale in protein-membrane interactions; however, these experiments can provide important information with relatively short experiment times and simple data analysis. This protocol will be especially useful in the Rainey lab as a tool to screen peptides before NMR spectroscopy experiments. NMR spectroscopy experiments can be expensive as they often require isotopically-labelled peptides in higher concentrations and deuterated solvents and surfactants. The experiments can also be very time-consuming, with complex data analysis; therefore, it is extremely useful to have a relatively inexpensive and efficient set of experiments to evaluate the peptide-micelle interactions and to identify peptides that may be of interest to further probe by NMR spectroscopy.

3.4. Summary

Fluorescence emission spectra for three pyrene-labelled isoforms of apelin were collected in the absence and presence of three different surfactant micelles: anionic SDS and LLPG, and zwitterionic DPC. *Py* values were calculated from the band I/band III ratio which showed that all three isoforms interact with the surfaces of both anionic, and zwitterionic surfactant micelles (Figure 3.13). Unlike previous studies by the Rainey lab (20), this technique did not indicate a weaker interaction between apelin and zwitterionic DPC micelles, compared to the anionic micelles. This could be explained by the larger dipole moment for the DPC headgroup compared to that of SDS or LPPG, which may have the effect of increasing the observed *Py* value. Overall, the results positively confirm an interaction between apelin and surfactant micelles, and have provided an efficient protocol for evaluating the interaction.

Table 3.1. *Py* values and standard error of the mean calculated from each fluorescence spectrum in the presence and absence of various surfactant micelles. All samples were 1 μmol/L in 20 mmol/L sodium phosphate buffer with 60 mmol/L NaCl, pH 7.0, analyzed at 37 °C. Surfactant concentration was 100 mmol/L. Spectra were collected in triplicate and *Py* values calculated for each repeat, then averaged.

	Buffer		**SDS**		**DPC**		**LPPG**	
Sample	Mean	*SEM*	Mean	*SEM*	Mean	*SEM*	Mean	*SEM*
Py-Cys-apelin-12	1.379	*0.025*	1.587	*0.002*	1.756	*0.013*	1.727	*0.039*
Py-Cys-apelin-17	1.450	*0.007*	1.790	*0.034*	1.777	*0.027*	1.854	*0.054*
Py-Cys-apelin-36	1.451	*0.044*	1.635	*0.039*	1.793	*0.028*	1.754	*0.010*
Py-mercaptoethanol	2.341	*0.056*	2.551	*0.025*	2.346	*0.010*	2.445	*0.022*
Pyrene	1.495	*0.060*	0.9866	*0.0365*	1.160	*0.055*	1.005	*0.048*

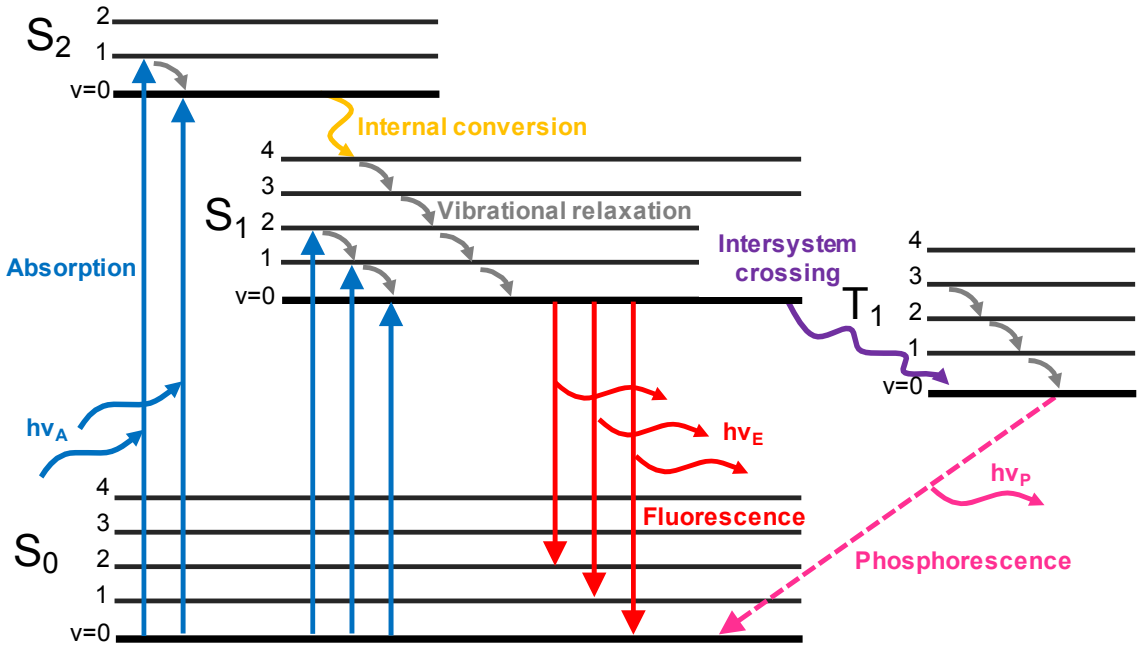

Figure 3.1. Jablonski diagram illustrating various forms of excitation and emission. Blue arrows indicate absorption of a photon and subsequent excitation from S_0 to S_1 or S_2. Orange arrow shows internal conversion from S_2 to S_1. Grey arrows indicate vibrational relaxation from $v>0$ to $v=0$. Red arrows indicate relaxation to S_0 and corresponding emission of a photon as fluorescence. Purple arrow indicates intersystem crossing from S_1 to T_1. Magenta arrow indicates relaxation from T_1 to S_0 and corresponding emission of a photon as phosphorescence.

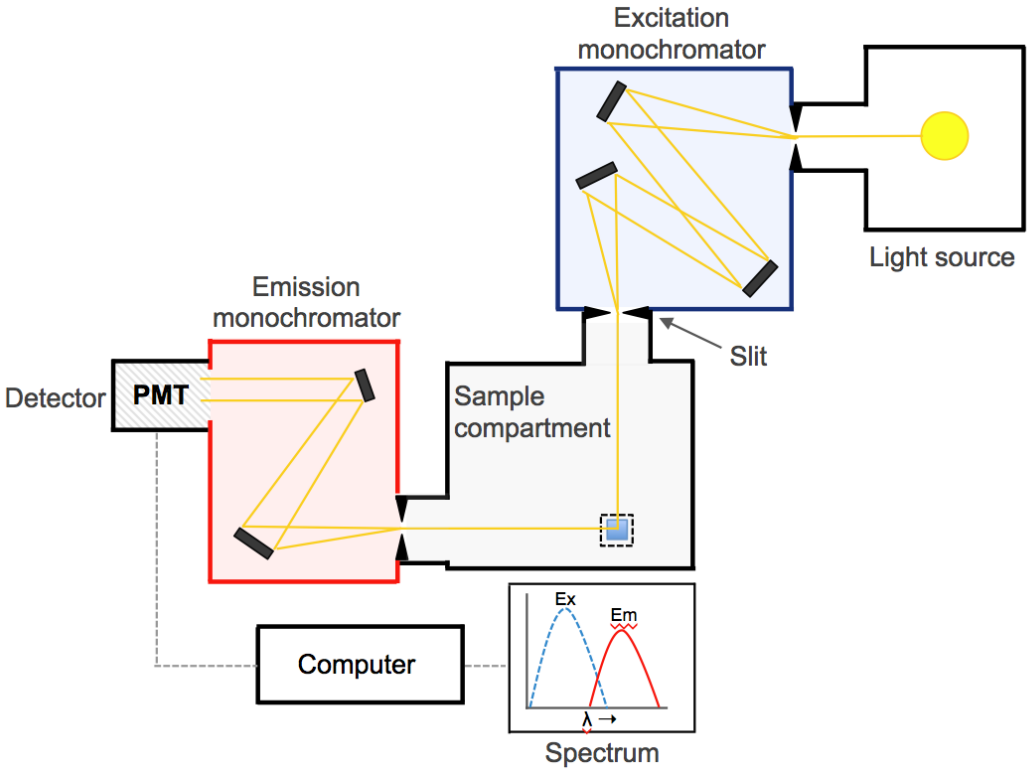

Figure 3.2. Schematic representation of a simplified spectrofluorometer instrument.

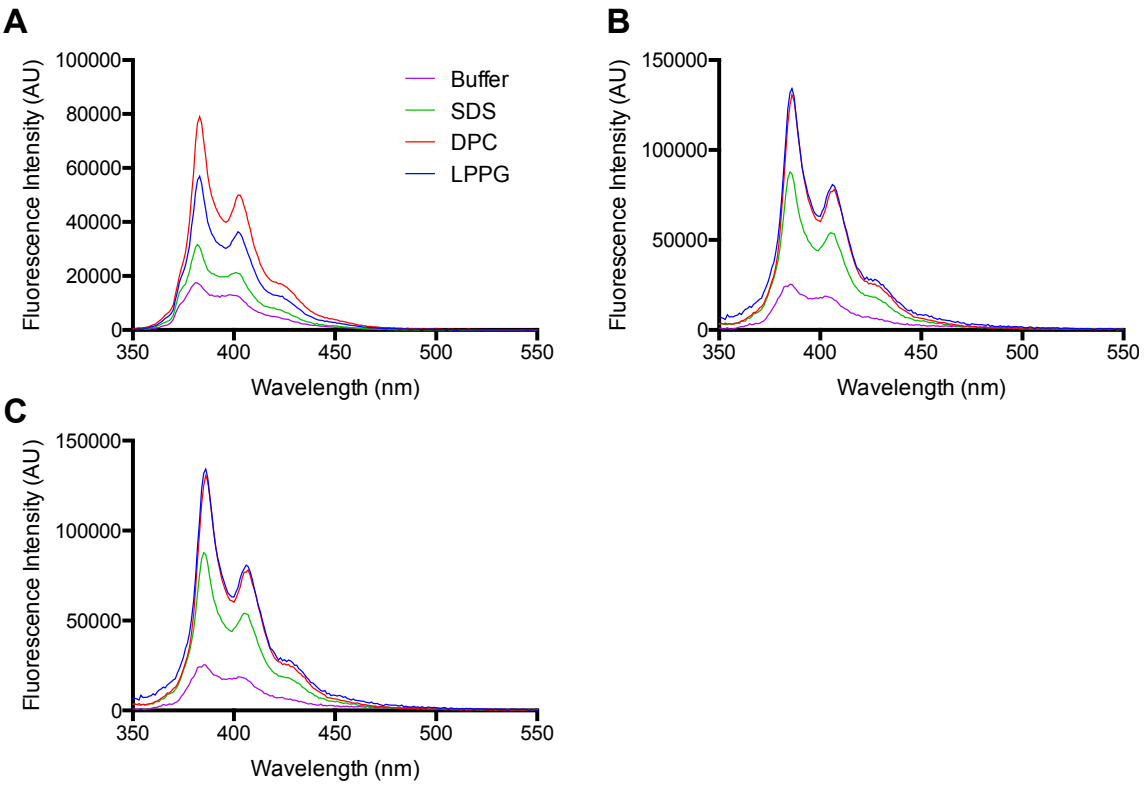

Figure 3.3. Fluorescence emission spectra of Py-Cys-apelin-12 (A), Py-Cys-apelin-17 (B), and Py-Cys-apelin-36 (C). 150 µL samples were 1 µmol/L peptide and 100 mmol/L surfactant in 20 mmol/L sodium phosphate buffer with 60 mmol/L NaCl at pH 7.0 analyzed at 37 °C. Both excitation and emission monochromators were set at 4 nm slit widths. The excitation wavelength was 340 nm and emission spectra were recorded from 350 nm – 550 nm with an integration time of 0.25 nm/s. Each experiment was repeated three times using fresh samples and spectra were averaged and blank subtracted.

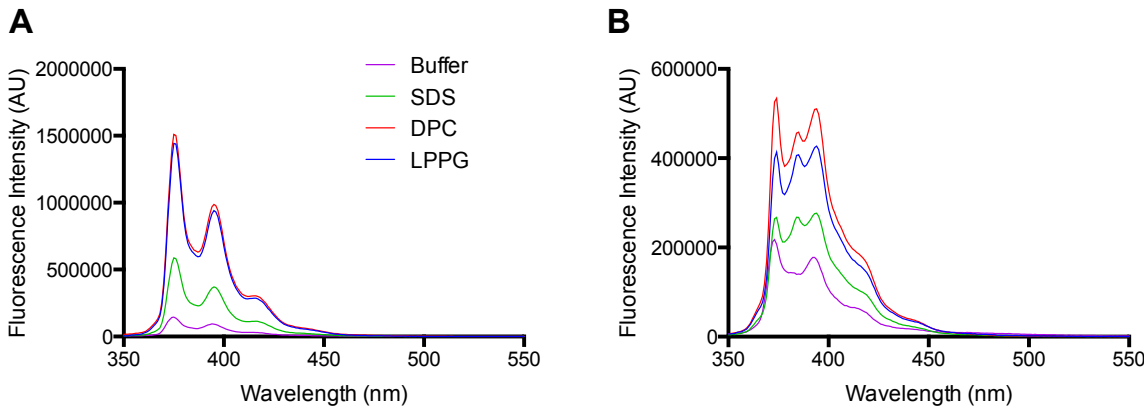

Figure 3.4. Fluorescence emission spectra of Py-mercaptoethanol (A) and pyrene (B). 150 µL samples were 1 µmol/L pyrene and 100 mmol/L surfactant in 20 mmol/L sodium phosphate buffer with 60 mmol/L NaCl at pH 7.0 analyzed at 37 °C. Both excitation and emission monochromators were set at 4 nm slit widths. The excitation wavelength was 340 nm and emission spectra were recorded from 350 nm – 550 nm with an integration time of 0.25 nm/s. Each experiment was repeated three times using fresh samples and spectra were averaged and blank subtracted.

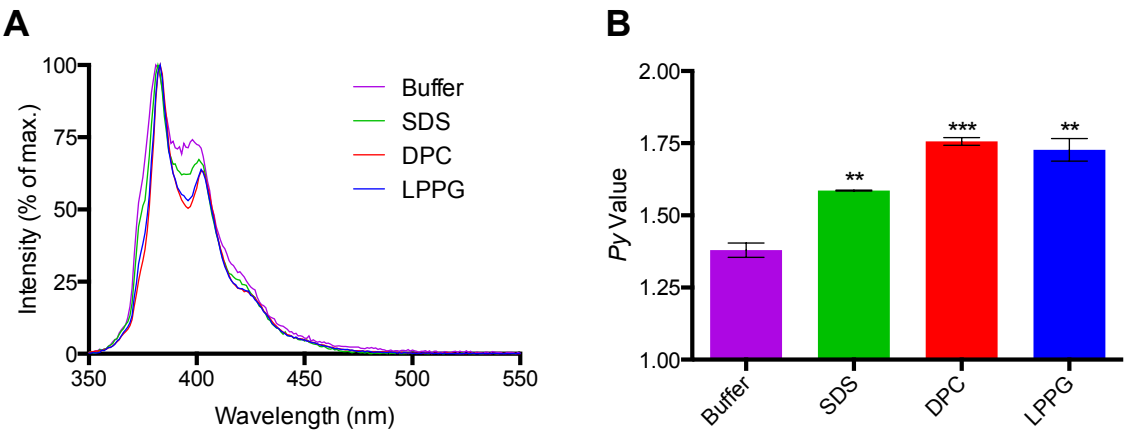

Figure 3.5. A) Normalized fluorescence emission spectra of Py-Cys-apelin-12. 150 µL samples were 1 µmol/L peptide and 100 mmol/L surfactant in 20 mmol/L sodium phosphate buffer with 60 mmol/L NaCl at pH 7.0 analyzed at 37 °C. Both excitation and emission monochromators were set at 4 nm slit widths. The excitation wavelength was 340 nm and emission spectra were recorded from 350 nm – 550 nm with an integration time of 0.25 nm/s. Each experiment was repeated three times using fresh samples and spectra were averaged and blank subtracted, then normalized to the maximum. B) *Py* values calculated from vibronic band I/III ratio from emission spectrum shown in (a). Surfactant values were compared to buffer value: $p \leq 0.01$, **; $p \leq 0.001$, ***.

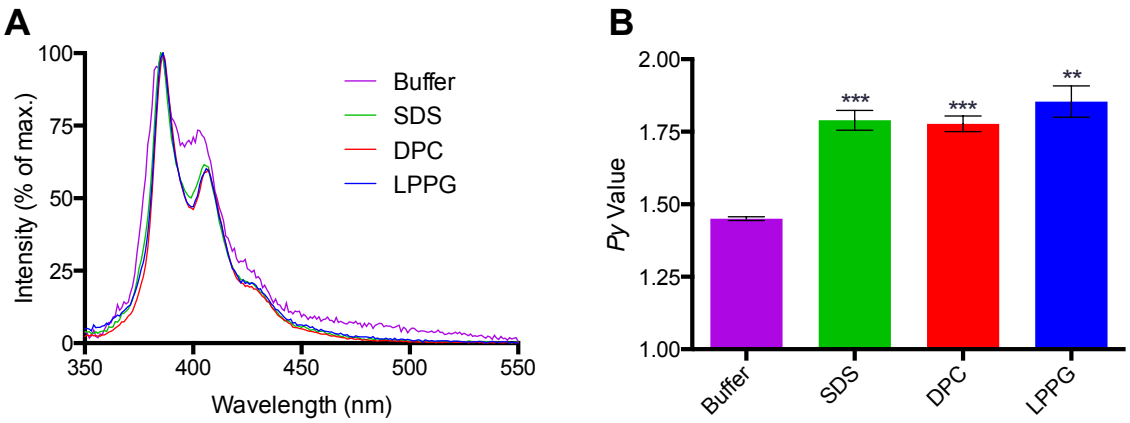

Figure 3.6. A) Normalized fluorescence emission spectra of Py-Cys-apelin-17. 150 µL samples were 1 µmol/L peptide and 100 mmol/L surfactant in 20 mmol/L sodium phosphate buffer with 60 mmol/L NaCl at pH 7.0 analyzed at 37 °C. Both excitation and emission monochromators were set at 4 nm slit widths. The excitation wavelength was 340 nm and emission spectra were recorded from 350 nm – 550 nm with an integration time of 0.25 nm/s. Each experiment was repeated three times using fresh samples and spectra were averaged and blank subtracted, then normalized to the maximum. B) *Py* values calculated from vibronic band I/III ratio from emission spectrum shown in (a). Surfactant values were compared to buffer value: $p \leq 0.01$, **; $p \leq 0.001$, ***.

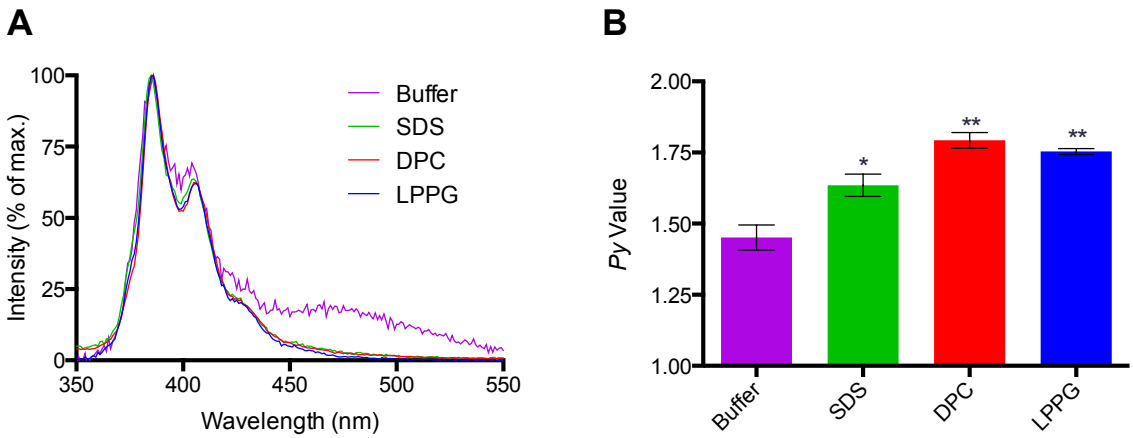

Figure 3.7. A) Normalized fluorescence emission spectra of Py-Cys-apelin-36. 150 µL samples were 1 µmol/L peptide and 100 mmol/L surfactant in 20 mmol/L sodium phosphate buffer with 60 mmol/L NaCl at pH 7.0 analyzed at 37 °C. Both excitation and emission monochromators were set at 4 nm slit widths. The excitation wavelength was 340 nm and emission spectra were recorded from 350 nm – 550 nm with an integration time of 0.25 nm/s. Each experiment was repeated three times using fresh samples and spectra were averaged and blank subtracted, then normalized to the maximum. B) *Py* values calculated from vibronic band I/III ratio from emission spectrum shown in (a). Surfactant values were compared to buffer value: $p \leq 0.05$, *; $p \leq 0.01$, **.

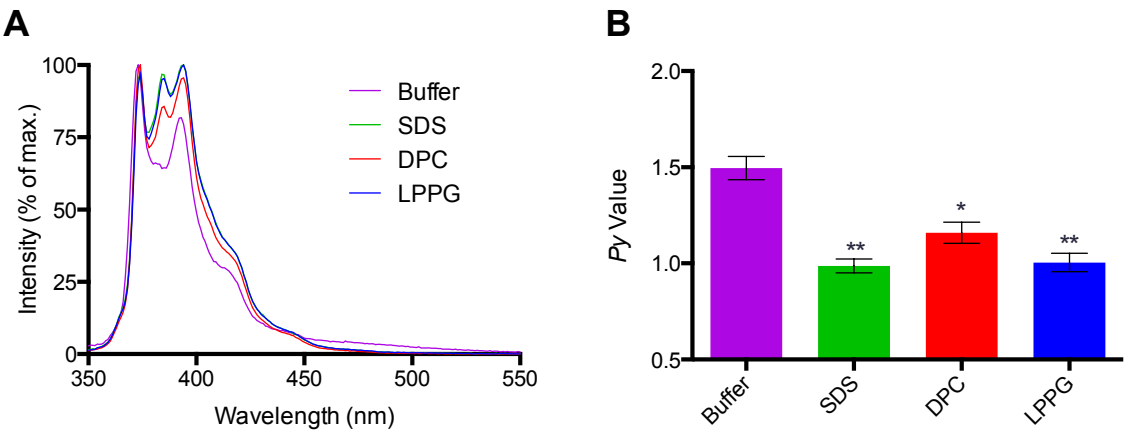

Figure 3.8. A) Normalized fluorescence emission spectra of pyrene. 150 µL samples were 1 µmol/L pyrene and 100 mmol/L surfactant in 20 mmol/L sodium phosphate buffer with 60 mmol/L NaCl at pH 7.0 analyzed at 37 °C. Both excitation and emission monochromators were set at 4 nm slit widths. The excitation wavelength was 340 nm and emission spectra were recorded from 350 nm – 550 nm with an integration time of 0.25 nm/s. Each experiment was repeated three times using fresh samples and spectra were averaged and blank subtracted, then normalized to the maximum. B) *Py* values calculated from vibronic band I/III ratio from emission spectrum shown in (a). Surfactant values were compared to buffer value: $p \leq 0.05$, *; $p \leq 0.01$, **.

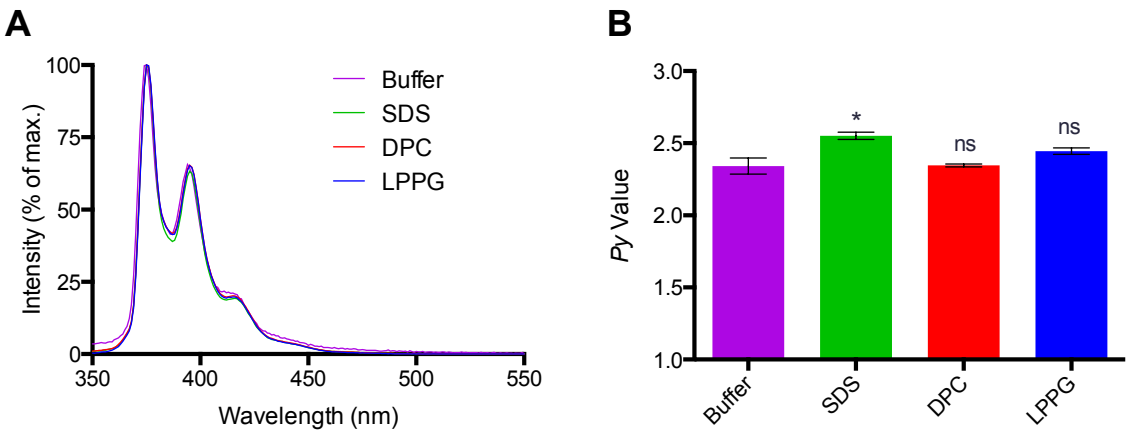

Figure 3.9. A) Normalized fluorescence emission spectra of Py-mercaptoethanol. 150 µL samples were 1 µmol/L pyrene and 100 mmol/L surfactant in 20 mmol/L sodium phosphate buffer with 60 mmol/L NaCl at pH 7.0 analyzed at 37 °C. Both excitation and emission monochromators were set at 4 nm slit widths. The excitation wavelength was 340 nm and emission spectra were recorded from 350 nm – 550 nm with an integration time of 0.25 nm/s. Each experiment was repeated three times using fresh samples and spectra were averaged and blank subtracted, then normalized to the maximum. B) *Py* values calculated from vibronic band I/III ratio from emission spectrum shown in (a). Surfactant values were compared to buffer value: $p>0.05$, not significant (ns); $p\leq 0.05$, *.

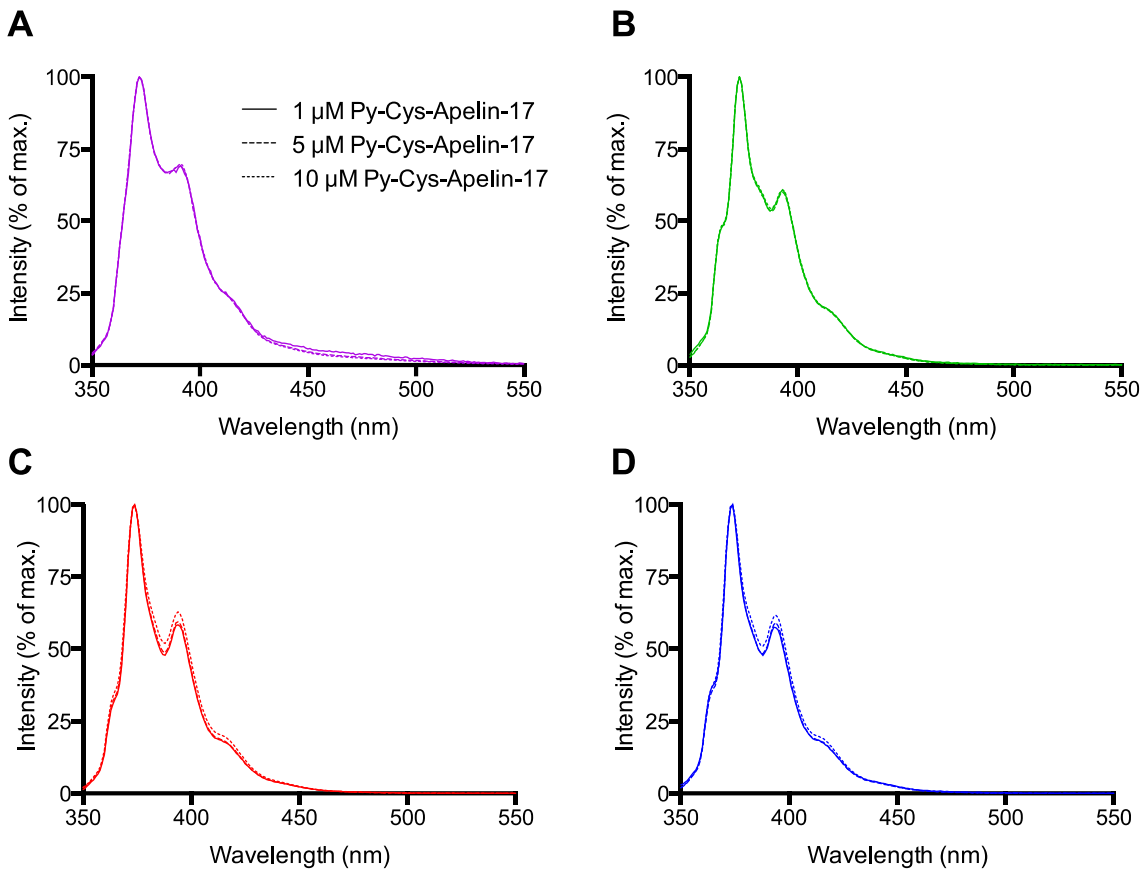

Figure 3.10. Fluorescence emission spectra of Py-Cys-apelin-17 in buffer (A), SDS (B), DPC (C), and LPPG (D). 150 µL samples ranged from 1 µmol/L to 10 µmol/L peptide and 100 mmol/L surfactant in 20 mmol/L sodium phosphate buffer with 60 mmol/L NaCl at pH 7.0 analyzed at 37 °C. Both excitation and emission monochromators were set at 4 nm slit widths. The excitation wavelength was 340 nm and emission spectra were recorded from 350 nm – 550 nm with an integration time of 0.25 nm/s. Each experiment was repeated three times using fresh samples and spectra were averaged and blank subtracted.

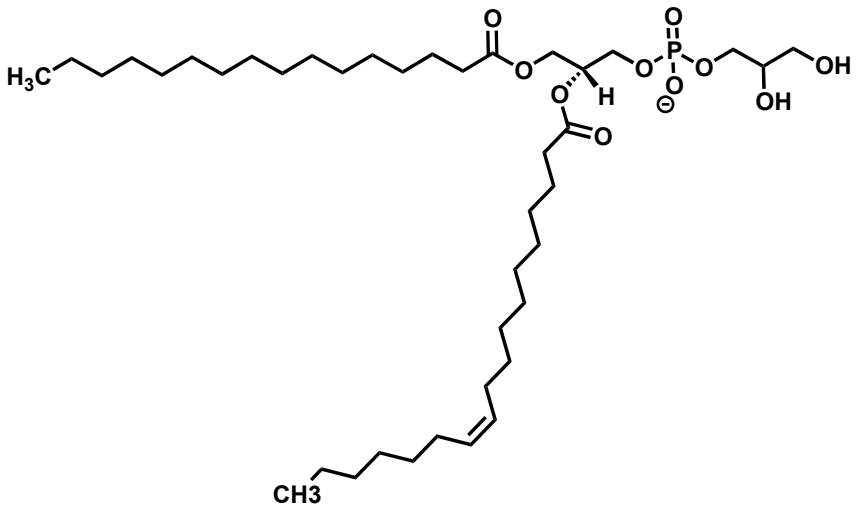

Figure 3.11. Chemical structure of [(1*R*)-1-[[[(2*S*)-2,3-dihydroxypropoxy]-hydroxy-phosphoryl]oxymethyl]-2-hexadecanoyloxy-ethyl] (*z*)-octadec-11-enoate.

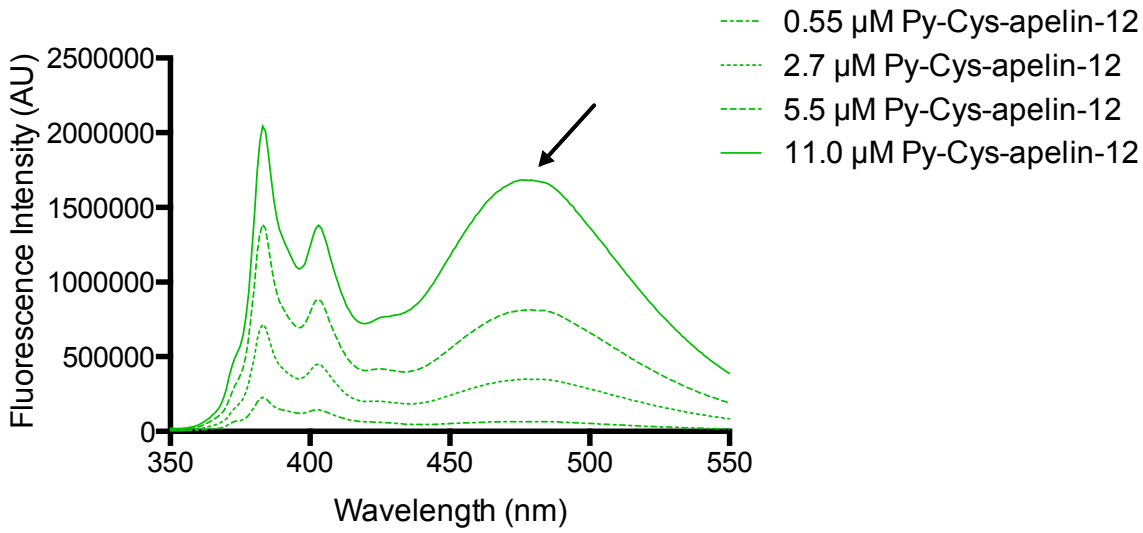

Figure 3.12. Fluorescence emission spectra of Py-Cys-apelin-12. 150 µL samples ranged from 0.55 µmol/L to 11 µmol/L peptide and 1 mmol/L SDS in 20 mmol/L sodium phosphate buffer with 60 mmol/L NaCl at pH 7.0 analyzed at 37 °C. Both excitation and emission monochromators were set at 4 nm slit widths. The excitation wavelength was 340 nm and emission spectra were recorded from 350 nm – 550 nm with an integration time of 0.25 nm/s. Each experiment was repeated three times using fresh samples and spectra were averaged and blank subtracted. Arrow indicates excimer band at ~475 nm.

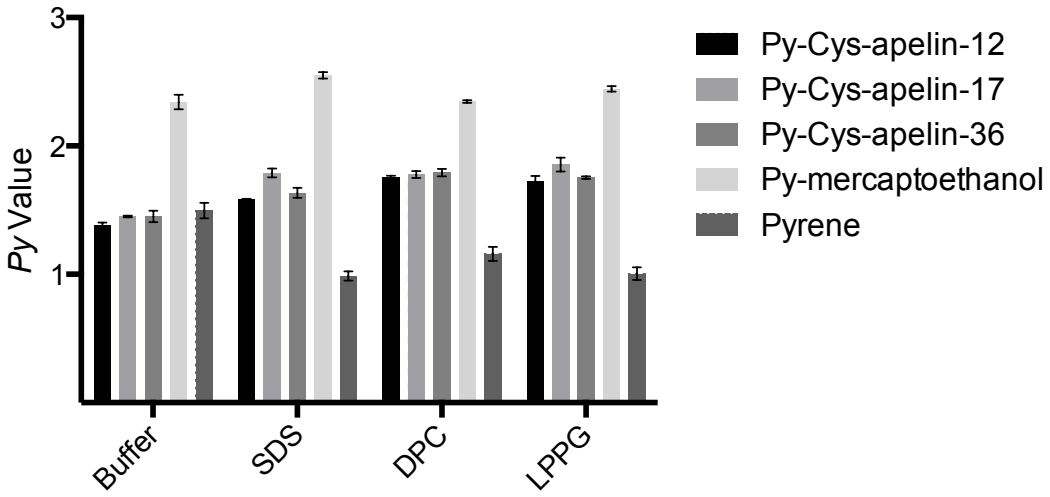

Figure 3.13. Summary of *Py* values calculated from vibronic band I/III ratio from emission spectra.

Chapter 4: Probing Ligand-Receptor Interactions with Förster Resonance Energy Transfer

4.1. Introduction

Förster (or fluorescence) resonance energy transfer (FRET) is a spectroscopic technique used to assess proximity and measure distances between and within fluorescent biomolecules. FRET is named for Professor Theodor Förster who first wrote about energy transfer in 1946 (73). FRET is the measure of energy transfer between a donor (D) fluorophore and an acceptor (A) fluorophore that are separated by a distance, r. FRET can be used to measure intermolecular distances between a D and A within a biomolecule, for example, the distances between two helices in a GPCR (74). FRET has also been used to examine the interaction between a protein and membrane lipids (75), and to detect ligand-receptor interactions (76). The possibilities for the use of FRET as a spectroscopic ruler are endless.

In order to exhibit FRET, an appropriate D and A pair (or FRET pair) must meet several criteria with respect to their spectroscopic properties. Firstly, the FRET pair must have overlapping emission and excitation spectra, meaning that the emission spectrum of the D must sufficiently overlap with the excitation spectrum of A to allow energy transfer to occur in that energy range. The degree of spectral overlap is defined by the overlap integral, J(λ):

$$J(\lambda) = \int_0^\infty F_D(\lambda)\varepsilon_A(\lambda)\lambda^4 d\lambda = \frac{\int_0^\infty F_D(\lambda)\varepsilon_A(\lambda)\lambda^4 d\lambda}{\int_0^\infty F_D(\lambda)d\lambda} \quad (4.1)$$

where $F_D(\lambda)$ is the baseline-corrected fluorescence intensity at λ and $\varepsilon_A(\lambda)$ is the extinction coefficient of the acceptor at λ, usually expressed in units of M^{-1} cm^{-1}. The second criterion required for FRET to occur is that the D and A must be within sufficiently close proximity, usually within 0-100 Å (77). The FRET donor must also have a high quantum yield and

relatively long lifetime. Tryptophan and pyrene are an appropriate FRET pair, as their emission and excitation spectra overlap: tryptophan absorbs in the regions 180-230 nm and 240-300 nm (40) and emits from 300-400 nm (78); pyrene absorbs strongly from 300-350 nm and emits from 375-410 nm (41) (Figure 4.1).

Each specific FRET pair will have a characteristic Förster distance (R_0) that is defined as the distance between D and A at which the FRET efficiency is 50%. At this distance, the number of photons emitted by D as fluorescence is 50% of the number of photons emitted as fluorescence in the absence of A. R_0 can be calculated from experimental measurements as follows:

$$R_0^6 = \frac{9000(\ln 10)\kappa^2 Q_D}{128\pi^5 N n^4} \int_0^\infty F_D(\lambda)\varepsilon_A(\lambda)\lambda^4 d\lambda = \frac{9000(\ln 10)\kappa^2 Q_D}{128\pi^5 N n^4} \cdot J(\lambda) \quad (4.2)$$

where κ^2 is a term that describes the orientation of the transition dipoles of the D and A with respect to each other (assumed to be equal to 2/3 in isotropic solution (79)); Q_D is the quantum yield of the donor; N is Avogadro's number; n is the refractive index of the medium (usually assumed to be equal to 1.4 for buffer solutions); and, J(λ) is as defined in equation 4.1. While it is possible to measure and calculate R_0, literature values for R_0 are available for many common FRET pairs. The literature R_0 value for tryptophan and pyrene is 28 Å (80). The FRET efficiency (E) is the fraction of photons that are absorbed by the donor that are then transferred to the acceptor, and is inversely proportional to the sixth power of distance, r, between D and A:

$$E = \frac{R_0^6}{R_0^6 + r^6} \quad (4.3)$$

E is also directly determinable from a fluorescence emission spectrum or lifetime measurement:

$$E = \frac{R_0^6}{R_0^6 + r^6} = 1 - \frac{\tau_{DA}}{\tau_D} = 1 - \frac{F_{DA}}{F_D} \quad (4.4)$$

where τ_{DA} is the lifetime of D in the presence of A; τ_D is the lifetime of D in the absence of A; F_{DA} is the fluorescence intensity of D in the presence of the acceptor; and, F_D is the fluorescence intensity of D in the absence of A. Therefore, by measuring the fluorescence emission of the tryptophan residues in AR55 in the absence and presence of increasing concentrations of pyrene-labelled apelin, it should be possible to estimate a distance between the tryptophan and pyrene using the R_0 value of 28 Å (Figure 4.2.) (80). During fluorescence experiments, tryptophan is typically excited at 290 nm; however, because AR55 also contains tyrosine, which also absorbs weakly at 290 nm, the FRET experiments discussed in this chapter use an excitation wavelength of 295 nm to avoid emission from tyrosine contributing to F_D measurements.

4.2. Materials and Methods

4.2.1. Materials

The pEXP5-CT vector was purchased from Invitrogen (Burlington, ON). Bacterial codon optimized AR55 and primers were purchased from Bio Basic Canada (Markham, ON). BL21(DE3) strain *E. coli* cells were purchased from Lucigen (Middleton, WI). Acetonitrile, ampicillin, IPTG, TFA and reagents for LB media were purchased from Fisher Scientific (Ottawa, ON). All other materials were purchased from Sigma-Aldrich Canada (Oakville, ON), unless otherwise stated.

4.2.2. Mutagenesis of AR55

The gene encoding AR55 was cloned into the pEXP5-CT vector by David Langelaan, immediately upstream of the 6xHis. The open reading frame encoding AR55-6xHis was mutated using QuikChange mutagenesis kit (Agilent Technologies Canada, Mississauga, ON) according to the conditions in Table 4.1. Single tryptophan residues were mutated to phenylalanine at positions W24 and W51 individually. Forward and reverse primers for the W24F mutation had the sequences 5'-AATATACCGATTTTAAAAGCAGCGGC-3' and 5'-GCCGCTGCTTTTAAAATCGGTATATT-3', respectively. Forward and reverse primers for the W51F mutation had the sequences 5'-CCTGGTGCTGTTTACCGTGTTTCG-3' and 5'-CGAAACACGGTAAACAGCACCAGG -3', respectively.

4.2.3. Expression of AR55 and AR55 Mutants

To express AR55, AR55-W24F, and AR55-W51F, the protocol for expression and purification developed by Langelaan *et al.* was followed (21). Briefly, the BL21(DE3) strain of *E. coli* was transformed with the pEXP5-CT vector containing the AR55 or mutated AR55 gene. The cells were grown for 16 h at 37 °C in a 250 mL Erlenmeyer flask containing 30 mL of LB medium with ampicillin (100 μg/mL). This culture was used to inoculate 2 L of LB medium with ampicillin (100 μg/mL), which was then grown to an optical density at 600 nm (OD_{600}) of 0.6. Expression was induced using IPTG (to a final concentration of 0.5 mmol/L). After induction, cells were grown for 4 h at 37 °C and harvested by centrifugation (6500g at 4 °C for 20 min). Cell pellets were resuspended in 30 mL lysis buffer (50 mmol/L NaH_2PO_4, 300 mmol/L NaCl, 10 mmol/L imidazole, titrated to pH 8.0 with NaOH) and the cells lysed using a French pressure cell press (American

Instrument Company, Silver Springs, MD). The lysate was centrifuged at 15,000g for 30 min at 4 °C.

4.2.4. Inclusion Body Purification

The pellet was resuspended in 25 mL wash buffer with Triton (50 mmol/L Tris-HCl, 0.5% Triton X-100, 100 mmol/L NaCl, 0.1% NaN_3, 10 mmol/L DTT, pH 8.0) using sonication. Centrifugation was carried out at 15,000g for 20 min at 4 °C. The supernatant was discarded and a second wash was repeated using wash buffer with Triton.

The pellet was resuspended in 25 mL wash buffer without Triton (50 mmol/L Tris-HCl, 1 mmol/L ethylenediaminetetraacetic acid sodium salt (EDTA-Na_2), 100 mmol/L NaCl, 0.1% NaN_3, 10 mmol/L DTT, pH 8.0) using sonication. Centrifugation was carried out at 15,000g for 20 min at 4 °C. The supernatant was discarded and a second wash was repeated using wash buffer without Triton. The final inclusion body pellet containing AR55 or mutated AR55 was resuspended in 10 mL 50% water (with 0.1% TFA) and 50% acetonitrile (with 0.1% TFA). The suspension was purified using RP-HPLC on a Prostar HPLC equipped with a diode array UV/Vis absorbance detector through monitoring of absorbance at 210 nm and 280 nm using a C_{18} matrix (5 μm particle, 20 mm x 250 mm Cosmosil column) with a water:acetonitrile (A:B) gradient with B progressing from 2 to 100% in 25 min at 8 mL/min flow rate. Product mass was confirmed using positive mode electrospray ionization mass spectrometry (Dalhousie Mass Spectrometry Laboratory, Halifax, NS).

4.2.5. Steady-State Fluorescent Spectroscopy FRET Experiments

All steady-state fluorescence spectroscopy FRET experiments were carried out on a Horiba Photon Technology International (Horiba PTI, London, ON) QuantaMaster-4CW

spectrofluorometer controlled using Felix32 software (PTI). Samples were analyzed in a 3 mm x 3 mm quartz microcuvette (Hellma Analytics) using 150 µL volumes at 37 °C. Both excitation and emission monochromators were set at 5 nm slit widths. Excitation wavelength (λ) for all FRET samples was 295 nm and emission spectra were recorded from 300 nm to 500 nm (for Py-Cys-apelin-17 concentrations ranging from 0 to 40 µmol/L) or 300 nm to 360 nm (for Py-Cys-apelin-17 concentrations greater than 40 µmol/L) with an integration time of 0.1 nm/s. Each experiment was repeated three times and spectra were averaged. Spectra were analyzed using GraphPad Prism (GraphPad Software).

An AR55 stock solution was made at a concentration of 150 µmol/L with a LPPG ratio of 1.5 micelles per peptide. Py-Cys-apelin-17 stock solution concentrations were 150 µmol/L and 1 mmol/L. Final samples were diluted to 20 µmol/L AR55 with 1.5 micelle to peptide ratio, and Py-Cys-apelin-17 concentrations increasing from 0 to 200 µmol/L in 20 mmol/L sodium phosphate buffer with 60 mmol/L NaCl at pH 7.0.

4.2.6. Calculation of FRET Efficiencies, Distances, and *Py* Values

FRET efficiencies (E) were calculated by selecting the tryptophan emission maximum around 300 nm – 330 nm for each spectrum. These values were then compared to the spectrum of AR55 in the absence of acceptor following equation 4.4. E values were analyzed using GraphPad prism, and fit to a one-phase association model:

$$Y = Y_0 + (Plateau - Y_0)(1 - e^{-Kx}) \quad (4.5)$$

where Y_0 is the Y (efficiency) value when X (Py-Cys-apelin-17 concentration) is 0, plateau is the Y value at infinite concentration, and K is the rate constant.

Distance values (r) were calculated using equation 4.4. *Py* values were calculated as described in Section 3.2.4.

4.3. Results and Discussion

In order to clearly distinguish between signals from the two native tryptophan residues in the AR55 sequence, these residues were substituted individually to obtain two single-tryptophan mutants of AR55. An existing pEXP5-CT vector containing the AR55-6xHis gene was successfully mutated using site-directed mutagenesis to individually substitute each of the two wild-type tryptophan residues to phenylalanine (AR55-W24F and AR55-W51F (Figure 1.4). Substitution of the tryptophan residues at the DNA level was confirmed by DNA sequencing. Expression of AR55 and AR55 mutant proteins was successfully induced with IPTG and inclusion body purification was monitored by SDS-PAGE (Figure 4.3). Each AR55 protein was purified from the inclusion body extract using RP-HPLC.

Steady-state fluorescence FRET experiments were successfully completed with Py-Cys-apelin-17 and WT AR55, AR55-W24F, and AR55-W51F in the presence of LPPG (Figure 4.4). It is not possible to distinguish between the two tryptophan residues in WT AR55 using steady-state fluorescence, therefore the experiments performed on WT AR55 were used simply for comparison. AR55 and LPPG concentrations were kept constant for all samples at 20 μmol/L and 3.75 mmol/L, respectively. An LPPG concentration of 3.75 mmol/L is still well above the CMC of 0.02 mmol/L, and corresponds to a micelle to peptide ratio of 1.5 assuming an aggregation number of 125 (81). Py-Cys-apelin-17 concentrations ranged from 1 μmol/L to 200 μmol/L, and these spectra were compared to those of AR55 in the absence of Py-Cys-apelin-17.

For each sample, the FRET efficiency (E) was calculated using the intensity at the tryptophan emission maximum (~300 nm – 330 nm) and comparing this to the intensity at the tryptophan emission maximum in the absence of Py-Cys-apelin-17 (Table 4.2). The

distance between tryptophan and pyrene (r) was calculated using equation 4.4, assuming a Förster distance (R_0) of 28 Å (80).

It was found that E increased with increasing Py-Cys-apelin-17 concentration for WT AR55, AR55-W24F, and AR55-W51F, indicating that the tryptophan and pyrene groups are in close enough proximity to allow for energy transfer. The relationship between E and Py-Cys-apelin-17 concentration can be described by a single-phase association exponential curve (Figure 4.5), with plateaus at ~0.9 for both AR55-W24F and AR55-W51F. E values calculated from Py-Cys-apelin-17 concentrations that are lower than saturation (i.e. <20 μmol/L) do not represent the true E, but rather an average of bound and unbound AR55; therefore, the corresponding r values calculated from these E values cannot be interpreted as true "distances". It is the r value calculated from the plateau of the E curve that best represents the actual distance between pyrene and tryptophan in a saturated system. These plateau r values were calculated to be ~20 Å for both AR55-W24F and AR55-W51F. When considering the position of the two tryptophan residues in the AR55 sequence, it was expected that AR55-W51F would display a shorter distance to pyrene compared to AR55-W24F because the remaining tryptophan at W24 is much closer to the two residues of the AR that have been shown to be essential for ligand binding (19), whereas W51 is located further away from this potential binding site, near the C-terminal end of the helix (21). From these calculations, it appears that the distance between pyrene and W24 is actually slightly greater than W51; however, it cannot be said definitively whether this difference is significant.

Another observation to consider is the blue shift in the tryptophan maximum emission wavelength. The maximum is shifted from 322 nm to 306 nm for AR55-W24F and from 321 nm to 303 nm for AR55-W51F (Figure 4.4). A blue shift in tryptophan fluorescence

emission indicates that the tryptophan residue is in a more hydrophobic environment (78). Tryptophan fluorescence is strongly affected by hydrogen bonding to the imino group. In a hydrophobic environment there is less hydrogen bonding, resulting in a shifted emission spectrum (78). An increase in hydrophobicity surrounding the tryptophan residue could be reasonably explained by ligand binding. Perhaps when apelin binds, the tryptophan becomes inserted further into the hydrophobic centre of the LPPG micelle due to a conformational change in AR55. This is a fair hypothesis because the two tryptophan residues are located very near the beginning and end of the helix, respectively (21). Along with a blue shift in emission, tryptophan residues also typically display an increase in fluorescence intensity in areas of greater hydrophobicity. If this is true for the current experiments, an increase in emission intensity upon ligand binding could in fact be obscuring the FRET calculations. Because these calculations are based on the intensity of the tryptophan band, without the effect of the hydrophobicity-related increase, the actual emission intensities may be significantly lower than what was observed, which would result in higher calculated FRET efficiencies and shorter r distances.

Py values were also calculated from the pyrene emission bands in the FRET experiments. It was found that the *Py* values for the lowest concentration of Py-Cys-apelin-17 (1 μmol/L) for all three AR55 samples were ~1.7 (Table 4.2). With increasing Py-Cys-apelin-17 concentrations, the *Py* value increased to ~1.9 for all three samples at 40 μmol/L. This trend of increasing *Py* value with increasing pyrene concentration was not observed in the peptide-micelle interaction experiments discussed in Section 3.3 (Figure 3.10). The values appear to increase very quickly from 1 μmol/L to 10 μmol/L, and then plateau at concentrations above 10 μmol/L. The most likely explanation is that this increase is actually an artefact caused by the overlapping tryptophan emission spectrum. Because the

tryptophan spectrum shows some emission at in the 385 nm – 395 nm region, this contribution to the pyrene bands likely affects the *Py* value calculation, whereas at higher concentrations of Py-Cys-apelin-17 where the pyrene emission is very strong, the contribution from tryptophan is negligible. Therefore, *Py* seems unlikely to be of use in understanding of these interactions.

In some experiments, it is possible to calculate FRET efficiencies from the increase in acceptor fluorescence, rather than the decrease in donor emission. However, it was found that pyrene absorbs quite strongly at the tryptophan excitation wavelength, 295 nm; therefore, background subtraction of pyrene emission due to direct excitation proved challenging. Pyrene also has such a high quantum yield that, at the concentrations required for binding experiments, fluorescence emission would be in a range that could be damaging to the instrument. To circumvent this issue, at Py-Cys-apelin-17 concentrations greater than 40 μmol/L, the emission spectra were monitored from 300 nm to 360 nm, instead of 300 nm to 500 nm, eliminating the range of pyrene emission. Therefore, it would not have been possible to obtain E values for those concentrations using the acceptor-based calculations.

Although FRET is a widely-used technique (79), and it has been used to investigate ligand-receptor interactions (76), there are currently no literature examples of the use of FRET to examine GPCR ligand binding sites. This chapter has demonstrated a unique example of using an extrinsic, small molecule fluorescent dye in combination with intrinsic, native tryptophan residues to probe the binding site between a segment of the AR and the cognate ligand, apelin.

4.4. Summary

FRET data were collected for the interaction between Py-Cys-apelin-17 and AR55, AR55-W24F, and AR55-W51F. All spectra showed a decrease in tryptophan emission with increased concentration of Py-Cys-apelin-17 (Figure 4.4). This decrease in F_D was used to calculate E and r from equation 4.4. Distance measurements for r showed an indistinguishable difference for W24 vs. W51, with both r values being ~20 Å. An increasing blue shift in tryptophan emission maximum with increasing Py-Cys-apelin-17 may indicate that upon ligand binding, the tryptophan residues are in a more hydrophobic environment, perhaps in the interior of the surfactant micelle or in a hydrophobic binding pocket created by apelin. This blue shift is typically accompanied by an increase in emission intensity, which could be effecting the E values calculated from F_{DA}. Overall, the results indicate that the pyrene group and tryptophan residues are within the range of FRET distance measurement upon binding, and further experiments may allow for distinguishable r values for the two tryptophan residues.

Table 4.1. The reaction composition and thermocycling conditions used for mutagenesis of AR55.

Reaction composition	
Buffer type and amount	1x Phusion HF reaction buffer, 10 μL
Template DNA (ng)	40
[Primers] (μmol/L)	0.2
dNTPs (μL)	1
Polymerase type and amount	Phusion, 1 U
Cycling conditions	
Initial denaturation	98 °C, 30 s
Number of cycles	25
Melting step	98 °C, 30 s
Annealing step	69 °C, 60 s
Extension step	72 °C, 3.5 min
Final extension	N/A

Table 4.1. FRET data showing energy transfer efficiency (E), and distance (r) for tryptophan in AR55 to pyrene in Py-Cys-apelin-17. *Py* values calculated from pyrene emission bands I/III. Plateau indicates values at infinite Py-Cys-apelin-17 concentration as calculated from equation 4.2.

	AR55			**AR55-W24F**			**AR55-W51F**		
Py-Cys-apelin-17 concentration	E	r	*Py*	E	r	*Py*	E	r	*Py*
0	0	-	-	0	-	-	0	-	-
1 μmol/L	0.0321	49.4	1.712	0.0618	44.1	1.657	0.0022	77.6	1.735
5 μmol/L	0.0574	44.6	1.872	0.172	36.4	1.850	0.0446	46.7	1.882
10 μmol/L	0.240	33.9	1.892	0.254	33.5	1.883	0.134	38.2	1.904
20 μmol/L	0.356	30.9	1.891	0.426	29.4	1.903	0.340	31.3	1.886
40 μmol/L	0.552	27.0	1.905	0.565	26.8	1.910	0.422	29.5	1.902
100 μmol/L	0.832	21.5		0.811	22.0		0.681	24.7	
200 μmol/L	0.943	17.6		0.928	18.3		0.882	20.0	
Plateau	0.941	17.7		0.891	19.7		0.884	19.9	

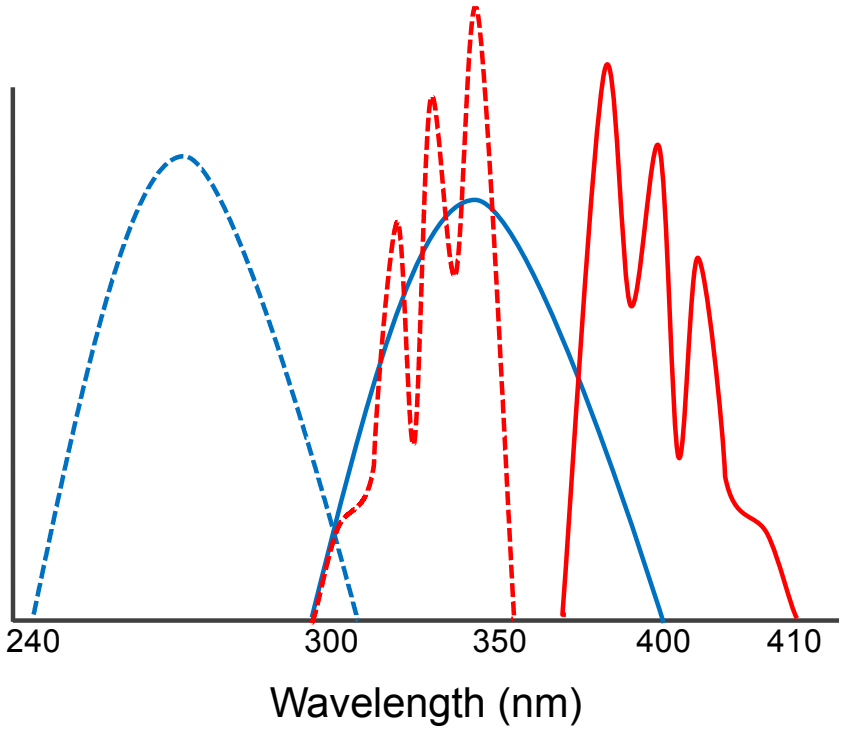

Figure 4.1. Schematic representation of the spectral overlap of tryptophan and pyrene. Tryptophan excitation spectrum shown as blue dashed line, tryptophan emission spectrum shown as blue solid line. Pyrene excitation spectrum shown as red dashed line, pyrene emission spectrum shown as red solid line.

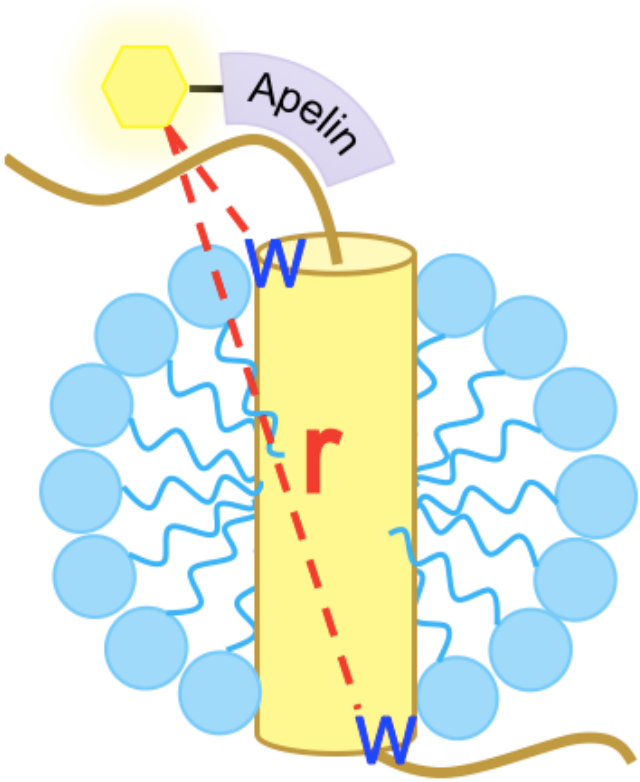

Figure 4.2. Schematic representation of FRET experiment between tryptophan residues of AR55 and pyrene-labelled apelin peptide. LPPG surfactant micelle shown in blue. AR55 helix and unstructured tails shown in brown. Tryptophan residues represented as blue Ws. Apelin is represented as grey rectangle, with pyrene represented as yellow hexagon. Distance between tryptophan and pyrene, r, shown as red dashed line.

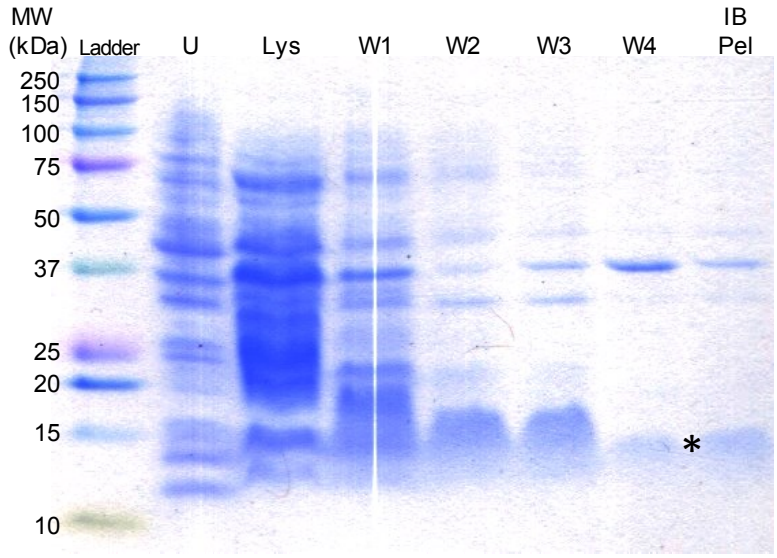

Figure 4.3. A 15% acrylamide SDS-PAGE after electrophoresis and Coommassie Blue staining showing initial expression and inclusion body purification of AR55. The protein ladder is shown on the left. U, uninduced; Lys, whole-cell lysate; W1-W5, inclusion body wash samples; IB Pel, inclusion body-containing pellet. AR55 is denoted by *.

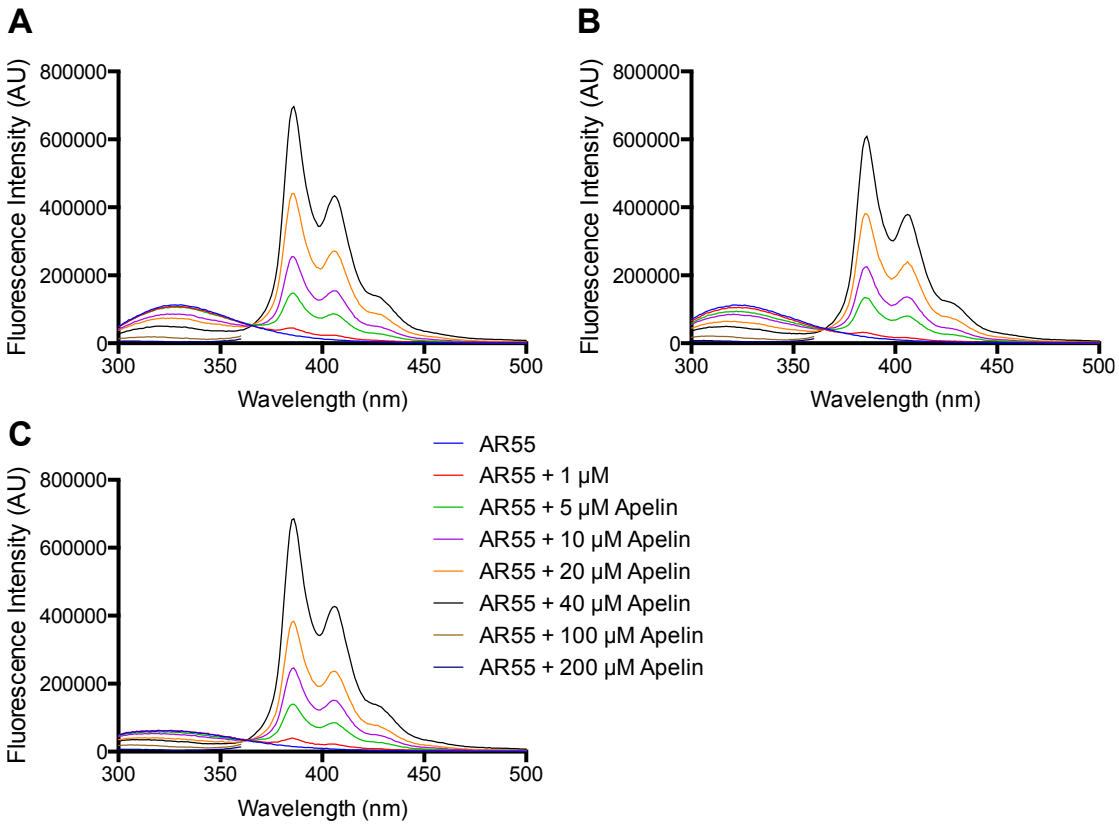

Figure 4.4. Fluorescence spectra of FRET experiments with Py-Cys-apelin-17 and AR55. 150 µL samples were 20 µmol/L AR55 (A), AR55-W24F (B), or AR55-W51F (C), with 1.5 LPPG micelle to AR55 ratio, and Py-Cys-apelin-17 concentrations increasing from 0 to 200 µmol/L in 20 mmol/L sodium phosphate buffer with 60 mmol/L NaCl at pH 7.0 analyzed at 37 °C. Both excitation and emission monochromators were set at 5 nm slit widths. Excitation wavelength for all FRET samples was 295 nm and emission spectra were recorded from 300 nm to 500 nm (for Py-Cys-apelin-17 concentrations ranging from 0 to 40 µmol/L) or 300 nm to 360 nm (for Py-Cys-apelin-17 concentrations greater than 40 µmol/L) with an integration time of 0.1 nm/s. Each experiment was repeated three times and spectra were averaged.

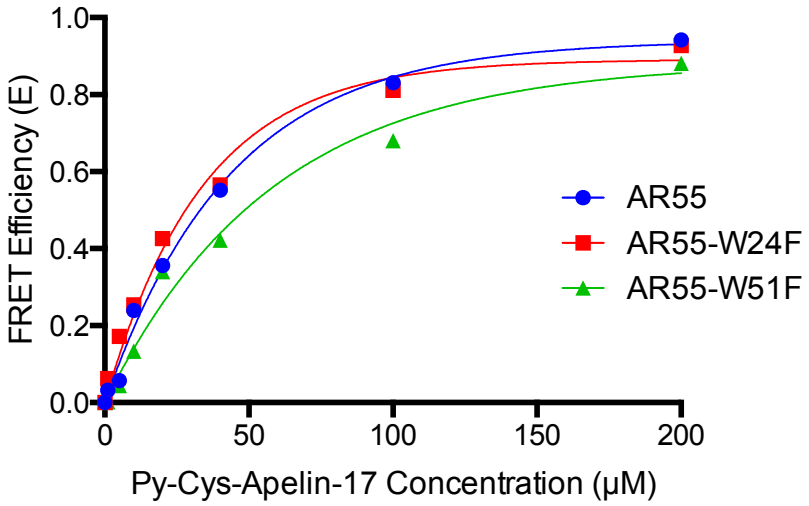

Figure 4.5. FRET E values (from Table 4.2) calculated from equation 4.4 and fit to the one-phase association model in equation 4.5.

Chapter 5: Conclusion

This work has demonstrated an efficient protocol for fluorescently-labelling apelin peptides (Chapter 2), and has shown two examples of the use of fluorophore-conjugated apelin isoforms and the valuable data that they can provide. In the first example outlined in Chapter 3, pyrene-labelled apelin isoforms were used to examine peptide interactions with membrane-mimetic surfactant micelles. The *Py* ratio calculated for each sample allowed for rapid evaluation of the interaction with both anionic and zwitterionic micelles. The most significant limitation of this technique is that it cannot provide a quantitative evaluation of the interaction between the peptide and surfactant micelle. Due to the effect of the dipole moment of the surfactant headgroups on the calculated *Py* values, the results are not representative of the strength or nature of the interactions. However, because of the simplicity and cost-effectiveness of this technique, it remains a useful tool to examine the membrane catalysis theory in combination with other, more complex experiments.

In the second example outlined in Chapter 4, the pyrene-labelled peptides were used to measure the distance between the pyrene group on the peptide and the tryptophan residues in the first TM segment of the AR. It was found that the pyrene group and tryptophan residues were within reasonable distance to measure FRET, however, it was not possible to distinguish between the results for each tryptophan residue. It should be noted that most published examples of FRET indicate relative distances, rather than absolute calculated distances (82-84). Based on these examples, it may not be possible to measure a discrete distance between pyrene and each tryptophan residue. However, with optimized conditions or perhaps a more appropriate acceptor fluorophore with spectral properties more similar to those of tryptophan, it should be possible to measure very precise relative distances for

each tryptophan residue. Collecting these measurements for an array of conditions involving all three apelin isoforms with various surfactant micelles of known sizes might allow for a more detailed description of the orientation of AR55 in the micelle, as well as the apelin binding site.

5.1. Future Work

Several different ideas for further examining apelin interactions have come out of this work. Most of these ideas centre around mutagenesis and determining the factors most strongly contributing to the interactions. It would be very interesting to synthesize scrambled apelin sequences to see if the micelle interaction is affected by calculating the corresponding *Py* value. If the *Py* value were to remain similar to native apelin sequences, it might indicate that the interaction is mostly due to the overall charge of the peptide, whereas if the *Py* value were to significantly change it might indicate that specific motifs within the sequence (for example the RPRL motif) are responsible for the interaction. If this were the case, it would be motivation to perform alanine scanning mutagenesis on the native apelin sequence to examine the contribution of each residue to the peptide-membrane interaction. Similar mutagenesis on the apelin sequence could also provide information about the binding between apelin and AR55 using FRET. Mutating regions of AR55 or important residues like E20 and D23, could also provide useful information about the binding interactions. Different fluorophores could also be conjugated to apelin using the same labelling technique to select different spectral ranges or properties that may further optimize the FRET experiments and allow for more precise distance measurements. A long-

term project goal would be to label apelin peptides with a fluorophore that is a FRET D or A for GFP to perform FRET experiments on full-length GFP-tagged AR in live cells.

Bibliography

1. Hall, R. A., Premont, R. T., and Lefkowitz, R. J. (1999) Heptahelical receptor signaling: Beyond the G protein paradigm. *J. Cell Biol.* **145**, 927–932

2. Overington, J. P., Al-Lazikani, B., and Hopkins, A. L. (2006) How many drug targets are there? *Nat. Rev. Drug Discov.* **5**, 993–996

3. Szokodi, I., Tavi, P., Földes, G., Voutilainen-Myllylä, S., Ilves, M., Tokola, H., Pikkaraimen, S., Piuhola, J., Rysä, J., Tóth, M., and Ruskoaho, H. (2002) Apelin, the novel endogenous ligand of the orphan receptor APJ, regulates cardiac contractility. *Circ. Res.* **91**, 434–440

4. Földes, G., Horkay, F., Szokodi, I., Vuolteenaho, O., Ilves, M., Lindstedt, K. A., Mäyränpää, M., Sármán, B., Seres, L., Skoumal, R., Lakó-Futó, Z., deChâtel, R., Ruskoaho, H., and Tóth, M. (2003) Circulating and cardiac levels of apelin, the novel ligand of the orphan receptor APJ, in patients with heart failure. *Biochem. Biophys. Res. Commun.* **308**, 480–485

5. Kleinz, M. J., and Davenport, A. P. (2005) Emerging roles of apelin in biology and medicine. *Pharmacol. Therapeut.* **107**, 198–211

6. Hosoya, M., Kawamata, Y., Fukusumi, S., Fujii, R., Habata, Y., Hinuma, S., Kitada, C., Honda, S., Kurokawa, T., Onda, H., Nishimura, O., and Fujino, M. (2000) Molecular and functional characteristics of APJ. Tissue distribution of mRNA and interaction with the endogenous ligand apelin. *J. Biol. Chem.* **275**, 21061–21067

7. Fan, X., Zhou, N., Zhang, X., Mukhtar, M., Lu, Z., Fang, J., DuBois, G. C., and Pomerantz, R. J. (2003) Structural and functional study of the apelin-13 peptide, an endogenous ligand of the HIV-1 coreceptor, APJ. *Biochemistry*. **42**, 10163–10168

8. Medhurst, A. D., Jennings, C. A., Robbins, M. J., Davis, R. P., Ellis, C., Winborn, K. Y., Lawrie, K. W. M., Hervieu, G., Riley, G., Bolaky, J. E., Herrity, N. C., Murdock, P., and Darker, J. G. (2003) Pharmacological and immunohistochemical characterization of the APJ receptor and its endogenous ligand apelin. *J. Neurochem.* **84**, 1162–1172

9. Lee, D. K., Saldivia, V. R., Nguyen, T., Cheng, R., George, S. R., and O'Dowd, B. F. (2005) Modification of the terminal residue of apelin-13 antagonizes its hypotensive action. *Endocrinology*. **146**, 231–236

10. Shin, K., Pandey, A., Liu, X.-Q., Anini, Y., and Rainey, J. K. (2013) Preferential apelin-13 production by the proprotein convertase PCSK3 is implicated in obesity. *FEBS Open Bio*. **3**, 328–333

11. Katugampola, S. D., Maguire, J. J., Matthewson, S. R., and Davenport, A. P. (2001) [125I]-(Pyr1)Apelin-13 is a novel radioligand for localizing the APJ orphan receptor in human and rat tissues with evidence for a vasoconstrictor role in man. *Brit. J. Pharmacol.* **132**, 1255–1260

12. Matsumoto, M., Hidaka, K., Akiho, H., Tada, S., Okada, M., and Yamaguchi, T. (1996) Low stringency hybridization study of the dopamine D4 receptor revealed D4-like mRNA distribution of the orphan seven-transmembrane receptor, APJ, in human brain. *Neurosci. Lett.* **219**, 119–122

13. Heinonen, M. V., Purhonen, A. K., Miettinen, P., Pääkkönen, M., Pirinen, E., Alhava, E., Åkerman, K., and Herzig, K. H. (2005) Apelin, orexin-A and leptin plasma levels in morbid obesity and effect of gastric banding. *Regul. Peptides*. **130**, 7–13

14. Zou, M.-X., Liu, H.-Y., Haraguchi, Y., Soda, Y., Tatemoto, K., and Hoshino, H. (2000) Apelin peptides block the entry of human immunodeficiency virus (HIV). *FEBS Lett.* **473**, 15–18

15. Han, R.-W., Xu, H.-J., Zhang, R.-S., and Wang, R. (2014) The role of apelin-13 in novel object recognition memory. *Peptides*. **62**, 155–158

16. Langelaan, D. N., Bebbington, E. M., Reddy, T., and Rainey, J. K. (2009) Structural insight into G-protein coupled receptor binding by apelin. *Biochemistry*. **48**, 537–548

17. Slupsky, C. M., Sykes, D. B., Gay, G. L., and Sykes, B. D. (2001) The HoxB1 hexapeptide is a prefolded domain: Implications for the Pbx1/Hox interaction. *Prot. Sci.* **10**, 1244–1253

18. Macaluso, N. J. M., and Glen, R. C. (2010) Exploring the "RPRL" motif of apelin-13 through molecular simulation and biological evaluation of cyclic peptide analogues. *ChemMedChem*. **5**, 1247–1253

19. Zhou, N., Zhang, X., Fan, X., Argyris, E., Fang, J., Acheampong, E., DuBois, G. C., and Pomerantz, R. J. (2003) The N-terminal domain of APJ, a CNS-based coreceptor for HIV-1, is essential for its receptor function and coreceptor activity. *Virology*. **317**, 84–94

20. Langelaan, D. N., and Rainey, J. K. (2009) Headgroup-dependent membrane catalysis of apelin-receptor interactions is likely. *J. Phys. Chem. B*. **113**, 10465–10471

21. Langelaan, D. N., Reddy, T., Banks, A. W., Dellaire, G., Dupré, D. J., and Rainey, J. K. (2013) Structural features of the apelin receptor N-terminal tail and first transmembrane segment implicated in ligand binding and receptor trafficking. *Biochim. Biophys. Acta*. **1828**, 1471–1483

22. Shoemaker, B. A., Portman, J. J., and Wolynes, P. G. (2000) Speeding molecular recognition by using the folding funnel: the fly-casting mechanism. *PNAS*. **97**, 8868–8873

23. Iturrioz, X., Gerbier, R., Leroux, V., Alvear-Perez, R., Maigret, B., and Llorens-Cortes, C. (2010) By interacting with the C-terminal Phe of apelin, Phe255 and Trp259 in helix VI of the apelin receptor are critical for internalization. *J. Biol. Chem.* **285**, 32627–32637

24. Langelaan, D. N., and Rainey, J. K. (2010) Membrane catalysis of peptide-receptor binding. *Biochem. Cell Biol.* **88**, 203–210

25. Sargent, D. F., and Schwyzer, R. (1986) Membrane lipid phase as catalyst for peptide-receptor interactions. *PNAS*. **83**, 5774–5778

26. Warschawski, D. E., Arnold, A. A., Beaugrand, M., Gravel, A., Chartrand, É., and Marcotte, I. (2011) Choosing membrane mimetics for NMR structural studies of transmembrane proteins. *Biochim. Biophys. Acta*. **1808**, 1957–1974

27. Chudakov, D. M., Matz, M. V., Lukyanov, S., and Lukyanov, K. A. (2010) Fluorescent proteins and their applications in imaging living cells and tissues. *Physiol. Rev.* **90**, 1103–1163

28. Zhang, J., Campbell, R. E., Ting, A. Y., and Tsien, R. Y. (2002) Creating new fluorescent probes for cell biology. *Nature Rev. Mol. Cell Biol*. **3**, 906–918

29. Prendergast, F. G., and Mann, K. G. (1978) Chemical and physical properties of aequorin and the green fluorescent protein isolated from Aequorea forskålea. *Biochemistry*. **17**, 3448–3453

30. Wu, Y.-W., and Goody, R. S. (2010) Probing protein function by chemical modification. *J. Pept. Sci.* **16**, 514–523

31. Murza, A., Besserer-Offroy, É., Côté, J., Bérubé, P., Longpré, J.-M., Dumaine, R., Lesur, O., Auger-Messier, M., Leduc, R., Sarret, P., and Marsault, É. (2015) C-Terminal modifications of apelin-13 significantly change ligand binding, receptor signaling, and hypotensive action. *J. Med. Chem.* **58**, 2431–2440

32. Panda, D., and Bhattacharyya, B. (1992) Excimer fluorescence of pyrene-maleimide-labeled tubulin. *Eur. J. Biochem.* **204**, 783–787

33. Han, M. K., Lin, P., Paek, D., Harvey, J. J., Fuior, E., and Knutson, J. R. (2002) Fluorescence studies of pyrene maleimide-labeled translin: excimer fluorescence indicates subunits associate in a tail-to-tail configuration to form octamer. *Biochemistry*. **41**, 3468–3476

34. Sahoo, D., Narayanaswami, V., Kay, C. M., and Ryan, R. O. (1998) Fluorescence studies of exchangeable apolipoprotein-lipid interactions. Superficial association of apolipophorin III with lipoprotein surfaces. *J. Biol. Chem.* **273**, 1403–1408

35. Wu, C. W., and Yarbrough, L. R. (1976) *N*-(1-pyrene)maleimide: A fluorescent cross-linking reagent. *Biochemistry*. **15**, 2863–2868

36. Awasthi, S. K., and Nielsen, P. E. (2002) Synthesis of PNA-peptide conjugates. in *Methods in Molecular Biology* (Vaidehi, N. ed), pp. 43–52, Humana Press, New Jersey, **208**, 43–52

37. Benoiton, N. L. (2006) *Chemistry of Peptide Synthesis*, Taylor and Francis, Boca Raton, Fla

38. Chan, W. C., and White, P. D. (2000) *Fmoc Solid Phase Peptide Synthesis* (Hames, B. D. ed), Oxford University Press, New York, NY

39. Roy, L. E., Hernández, C. E., and Acree, W. E., Jr (1999) Thermodynamics of Mobile Order Theory. Part 3. Comparison of experimental and predicted solubilities for fluoranthene and pyrene. *Polycycl Aromat Comp*. **13**, 205–219

40. Schmid, F. X. (2001) *Biological Macromolecules: UV-visible Spectrophotometry*, John Wiley & Sons, Ltd, Chichester, UK

41. Bains, G., Patel, A. B., and Narayanaswami, V. (2011) Pyrene: A probe to study protein conformation and conformational changes. *Molecules*. **16**, 7909–7935

42. Lakowicz, J. R. (2006) Introduction to Fluorescence. in *Principles of Fluorescence Spectroscopy*, 3rd Ed., Springer, New York, NY

43. Lakowicz, J. R. (2006) Fluorophores. in *Principles of Fluorescence Spectroscopy*, 3rd Ed., Springer, New York, NY

44. Bai, B., Jiang, Y., Cai, X., and Chen, J. (2014) Dynamics of apelin receptor/G protein coupling in living cells. *Exp. Cell. Res.* **328**, 401–409

45. Kraynov, V. S. (2000) Localized Rac activation dynamics visualized in living cells. *Science*. **290**, 333–337

46. Patel, A. B., Khumsupan, P., and Narayanaswami, V. (2010) Pyrene fluorescence analysis offers new insights into the conformation of the lipoprotein-binding domain of human apolipoprotein E. *Biochemistry*. **49**, 1766–1775

47. Jabłoński, A. (1935) Über den Mechanismus der Photolumineszenz von Farbstoffphosphoren. *Z. Physik*. **94**, 38–46

48. Stokes, G. G. (1852) On the change of refrangibility of light. *Philos. T. R. Soc. Lond*. **142**, 463–562

49. Lakowicz, J. R. (2006) Instrumentation for Fluorescence Spectroscopy. in *Principles of Fluorescence Spectroscopy*, 3rd Ed., Springer, New York, NY

50. Nakajima, A. (1971) Solvent effect on the vibrational structures of the fluorescence and absorption spectra of pyrene. *B. Chem. Soc. Jpn.* **44**, 3272–3277

51. Kalyanasundaram, K., and Thomas, J. K. (1977) Environmental effects on vibronic band intensities in pyrene monomer fluorescence and their application in studies of micellar systems. *J. Am. Chem. Soc.* **99**, 2039–2044

52. Karpovich, D. S., and Blanchard, G. J. (1995) Relating the polarity-dependent fluorescence response of pyrene to vibronic coupling. Achieving a fundamental understanding of the py polarity scale. *J. Phys. Chem.* **99**, 3951–3958

53. Reichardt, C. C., and Welton, T. T. (2011) Solvent Effects on the Absorption Spectra of Organic Compounds. in *Solvents and Solvent Effects in Organic Chemistry*, 4 Ed. (Welton, T. T. ed), Wiley-VCH, Weinheim, Germany

54. Dong, D. C., and Winnik, M. A. (1982) Solvent effects on the vibronic fine structure of pyrene fluorescence and empirical correlations with ET and Y values. *Photochem. Photobiol*. **35**, 17–21

55. Dong, D. C., and Winnik, M. A. (1984) The Py scale of solvent polarities. *Can. J. Chem*. **62**, 2560–2565

56. Tamamizu-Kato, S., Kosaraju, M. G., Kato, H., Raussens, V., Ruysschaert, J.-M., and Narayanaswami, V. (2006) Calcium-triggered membrane interaction of the alpha-synuclein acidic tail. *Biochemistry*. **45**, 10947–10956

57. Stevens, B., and Hutton, E. (1960) Radiative life-time of the pyrene dimer and the possible role of excited dimers in energy transfer processes. *Nature*. **186**, 1045–1046

58. Birks, J. B. (1975) Excimers. *Rep. Prog. Phys.* **38**, 903–974

59. Bains, G. K., Kim, S. H., Sorin, E. J., and Narayanaswami, V. (2012) The extent of pyrene excimer fluorescence emission is a reflector of distance and flexibility: Analysis of the segment linking the LDL receptor-binding and tetramerization domains of apolipoprotein E3. *Biochemistry*. **51**, 6207–6219

60. Sahoo, D., Weers, P. M. M., Ryan, R. O., and Narayanaswami, V. (2002) Lipid-triggered conformational switch of apolipophorin III helix bundle to an extended helix organization. *J. Mol. Biol.* **321**, 201–214

61. Basu Ray, G., Chakraborty, I., and Moulik, S. P. (2006) Pyrene absorption can be a convenient method for probing critical micellar concentration (cmc) and indexing micellar polarity. *J. Colloid Interf. Sci.* **294**, 248–254

62. Atik, S. S., Nam, M., and Singer, L. A. (1979) Transient studies on intramicellar excimer formation. A useful probe of the host micelle. *Chem Phys Lett*. **67**, 75–80

63. Lianos, P., and Zana, R. (1980) Use of pyrene excimer formation to study the effect of sodium chloride on the structure of sodium dodecyl sulfate micelles. *J. Phys. Chem.* **84**, 3339–3341

64. Haugland, R. P. (1996) *Handbook of Fluorescent Probes and Research Chemicals*, Molecular Probes Inc, Eugene, OR

65. Lakowicz, J. R. (2006) *Principles of Fluorescence Spectroscopy*, 3rd Ed., Springer, New York, NY

66. Winkler, M. H. (1967) Some notes on fluorescence intensity. *Biophys. J.* **7**, 719–725

67. Sauer, M., Hofkens, J., and Enderlein, J. (2010) Basic Principles of Fluorescence Spectroscopy. in *Handbook of Fluorescence Spectroscopy and Imaging*, Wiley-VCH, Weinheim, Germany

68. Paul, B. C., lslam, S. S., and Ismail, K. (1998) Effect of acetate and propionate co-ions on the micellization of sodium dodecyl sulfate in water. *J. Phys. Chem. B*. **102**, 7807–7812

69. Stafford, R. E., Fanni, T., and Dennis, E. A. (1989) Interfacial properties and critical micelle concentration of lysophospholipids. *Biochemistry*. **28**, 5113–5120

70. Hutchison, G. R., and Lambrecht, D. S. Pitt Quantum Repository. doi: 10.17614/Q4MS5W. Retrieved from http://pqr.pitt.edu/mol/QBHFVMDLPTZDOI-UHFFFAOYSA-N

71. Hutchison, G. R., and Lambrecht, D. S. Pitt Quantum Repository. doi: 10.17614/Q46970V28. Retrieved from http://pqr.pitt.edu/mol/DBMJMQXJHONAFJ-UHFFFAOYSA-M

72. Hutchison, G. R., and Lambrecht, D. S. Pitt Quantum Repository. doi: 10.17614/Q4TB0ZJ5J. Retrieved from http://pqr.pitt.edu/mol/ADYWCMPUNIVOEA-GPJPVTGXSA-N

73. Förster, T. (1946) Energiewanderung und Fluoreszenz. *Naturwissenschaften*. **33**, 166–175

74. Thévenin, D., and Lazarova, T. (2012) Identifying and measuring transmembrane helix-helix interactions by FRET. in *Methods in Molecular Biology* (Vaidehi, N., and Klein-Seetharaman, J. eds), pp. 87–106, Humana Press, Totowa, NJ, **914**, 87–106

75. Suárez-Germà, C., Hernández-Borrell, J., Prieto, M., and Loura, L. M. S. (2014) Modeling FRET to investigate the selectivity of lactose permease of Escherichia coli for lipids. *Mol. Membr. Biol.* **31**, 120–130

76. Louie, A. Y., and Tromberg, B. J. (1998) Fluorescence resonance energy transfer: FRET studies of ligand binding to cell surface receptors. *J. Fluoresc.* **8**, 13–20

77. Hussain, S. A. (2009) An Introduction to Fluorescence Resonance Energy Transfer (FRET). *arXiv:0908.1815 [physics.gen-ph]*

78. Lakowicz, J. R. (2006) Protein Fluorescence. in *Principles of Fluorescence Spectroscopy*, Springer, New York, NY

79. Lakowicz, J. R. (2006) Energy Transfer. in *Principles of Fluorescence Spectroscopy*, 3rd Ed., Springer, New York, NY

80. Wu, P., and Brand, L. (1994) Resonance energy transfer: methods and applications. *Anal. Biochem.* **218**, 1–13

81. Jan Lipfert, Linda Columbus, Vincent B Chu, Scott A Lesley, A., Sebastian Doniach (2007) Size and shape of detergent micelles determined by small-angle X-ray scattering. *J. Phys. Chem. B*. **111**, 12427–12438

82. Ivan Rasnik, Sean A McKinney, A., Taekjip Ha (2005) Surfaces and orientations: Much to FRET about? *Acc. Chem. Res.* **38**, 542–548

83. Maity, A., Mukherjee, P., Das, T., Ghosh, P., and Purkayastha, P. (2012) Förster resonance energy transfer between pyrene and bovine serum albumin: Effect of the hydrophobic pockets of cyclodextrins. *Spectrochim. Acta A*. **92**, 382–387

84. Mote, U. S., Patil, S. R., Bhosale, S. H., Han, S. H., and Kolekar, G. B. (2011) Fluorescence resonance energy transfer from tryptophan to folic acid in micellar media and deionised water. *J. Photoch. Photobio. B*. **103**, 16–21

Appendix i: License for Figure 1.2

RightsLink®

Home | Create Account | Help | Live Chat

Title:	Structural Insight into G-Protein Coupled Receptor Binding by Apelin†
Author:	David N. Langelaan, E. Meghan Bebbington, Tyler Reddy, et al
Publication:	Biochemistry
Publisher:	American Chemical Society
Date:	Jan 1, 2009

LOGIN

If you're a copyright.com user, you can login to RightsLink using your copyright.com credentials. Already **a RightsLink user** or want to learn more?

PERMISSION/LICENSE IS GRANTED FOR YOUR ORDER AT NO CHARGE

This type of permission/license, instead of the standard Terms & Conditions, is sent to you because no fee is being charged for your order. Please note the following:

- Permission is granted for your request in both print and electronic formats, and translations.
- If figures and/or tables were requested, they may be adapted or used in part.
- Please print this page for your records and send a copy of it to your publisher/graduate school.
- Appropriate credit for the requested material should be given as follows: "Reprinted (adapted) with permission from (COMPLETE REFERENCE CITATION). Copyright (YEAR) American Chemical Society." Insert appropriate information in place of the capitalized words.
- One-time permission is granted only for the use specified in your request. No additional uses are granted (such as derivative works or other editions). For any other uses, please submit a new request.

If credit is given to another source for the material you requested, permission must be obtained from that source.

BACK | CLOSE WINDOW

Appendix ii: License for Figure 1.5

ELSEVIER LICENSE
TERMS AND CONDITIONS

Nov 16, 2015

This is a License Agreement between Robin Patterson ("You") and Elsevier ("Elsevier") provided by Copyright Clearance Center ("CCC"). The license consists of your order details, the terms and conditions provided by Elsevier, and the payment terms and conditions.

All payments must be made in full to CCC. For payment instructions, please see information listed at the bottom of this form.

Supplier	Elsevier Limited The Boulevard,Langford Lane Kidlington,Oxford,OX5 1GB,UK
Registered Company Number	1982084
Customer name	Robin Patterson
Customer address	5850 College Street Halifax, NS B3H 4R2
License number	3750930637780
License date	Nov 16, 2015
Licensed content publisher	Elsevier
Licensed content publication	Biochimica et Biophysica Acta (BBA) - Biomembranes
Licensed content title	Structural features of the apelin receptor N-terminal tail and first transmembrane segment implicated in ligand binding and receptor trafficking
Licensed content author	David N. Langelaan,Tyler Reddy,Aaron W. Banks,Graham Dellaire,Denis J. Dupré,Jan K. Rainey
Licensed content date	June 2013
Licensed content volume number	1828
Licensed content issue number	6
Number of pages	13
Start Page	1471
End Page	1483
Type of Use	reuse in a thesis/dissertation
Portion	figures/tables/illustrations
Number of figures/tables/illustrations	1
Format	both print and electronic
Are you the author of this Elsevier article?	No

Will you be translating?	No
Original figure numbers	Figure 3c
Title of your thesis/dissertation	Probing Membrane Catalyzed Apelin-Receptor Interactions by Fluorescence Spectroscopy
Expected completion date	Dec 2015
Estimated size (number of pages)	100
Elsevier VAT number	GB 494 6272 12
Permissions price	0.00 CAD
VAT/Local Sales Tax	0.00 CAD / 0.00 GBP
Total	0.00 CAD
Terms and Conditions	

INTRODUCTION

1. The publisher for this copyrighted material is Elsevier. By clicking "accept" in connection with completing this licensing transaction, you agree that the following terms and conditions apply to this transaction (along with the Billing and Payment terms and conditions established by Copyright Clearance Center, Inc. ("CCC"), at the time that you opened your Rightslink account and that are available at any time at http://myaccount.copyright.com).

GENERAL TERMS

2. Elsevier hereby grants you permission to reproduce the aforementioned material subject to the terms and conditions indicated.
3. Acknowledgement: If any part of the material to be used (for example, figures) has appeared in our publication with credit or acknowledgement to another source, permission must also be sought from that source. If such permission is not obtained then that material may not be included in your publication/copies. Suitable acknowledgement to the source must be made, either as a footnote or in a reference list at the end of your publication, as follows:
"Reprinted from Publication title, Vol /edition number, Author(s), Title of article / title of chapter, Pages No., Copyright (Year), with permission from Elsevier [OR APPLICABLE SOCIETY COPYRIGHT OWNER]." Also Lancet special credit - "Reprinted from The Lancet, Vol. number, Author(s), Title of article, Pages No., Copyright (Year), with permission from Elsevier."
4. Reproduction of this material is confined to the purpose and/or media for which permission is hereby given.
5. Altering/Modifying Material: Not Permitted. However figures and illustrations may be altered/adapted minimally to serve your work. Any other abbreviations, additions, deletions and/or any other alterations shall be made only with prior written authorization of Elsevier Ltd. (Please contact Elsevier at permissions@elsevier.com)
6. If the permission fee for the requested use of our material is waived in this instance, please be advised that your future requests for Elsevier materials may attract a fee.
7. Reservation of Rights: Publisher reserves all rights not specifically granted in the combination of (i) the license details provided by you and accepted in the course of this licensing transaction, (ii) these terms and conditions and (iii) CCC's Billing and Payment terms and conditions.
8. License Contingent Upon Payment: While you may exercise the rights licensed immediately upon issuance of the license at the end of the licensing process for the transaction, provided that you have disclosed complete and accurate details of your proposed

use, no license is finally effective unless and until full payment is received from you (either by publisher or by CCC) as provided in CCC's Billing and Payment terms and conditions. If full payment is not received on a timely basis, then any license preliminarily granted shall be deemed automatically revoked and shall be void as if never granted. Further, in the event that you breach any of these terms and conditions or any of CCC's Billing and Payment terms and conditions, the license is automatically revoked and shall be void as if never granted. Use of materials as described in a revoked license, as well as any use of the materials beyond the scope of an unrevoked license, may constitute copyright infringement and publisher reserves the right to take any and all action to protect its copyright in the materials.

9. Warranties: Publisher makes no representations or warranties with respect to the licensed material.

10. Indemnity: You hereby indemnify and agree to hold harmless publisher and CCC, and their respective officers, directors, employees and agents, from and against any and all claims arising out of your use of the licensed material other than as specifically authorized pursuant to this license.

11. No Transfer of License: This license is personal to you and may not be sublicensed, assigned, or transferred by you to any other person without publisher's written permission.

12. No Amendment Except in Writing: This license may not be amended except in a writing signed by both parties (or, in the case of publisher, by CCC on publisher's behalf).

13. Objection to Contrary Terms: Publisher hereby objects to any terms contained in any purchase order, acknowledgment, check endorsement or other writing prepared by you, which terms are inconsistent with these terms and conditions or CCC's Billing and Payment terms and conditions. These terms and conditions, together with CCC's Billing and Payment terms and conditions (which are incorporated herein), comprise the entire agreement between you and publisher (and CCC) concerning this licensing transaction. In the event of any conflict between your obligations established by these terms and conditions and those established by CCC's Billing and Payment terms and conditions, these terms and conditions shall control.

14. Revocation: Elsevier or Copyright Clearance Center may deny the permissions described in this License at their sole discretion, for any reason or no reason, with a full refund payable to you. Notice of such denial will be made using the contact information provided by you. Failure to receive such notice will not alter or invalidate the denial. In no event will Elsevier or Copyright Clearance Center be responsible or liable for any costs, expenses or damage incurred by you as a result of a denial of your permission request, other than a refund of the amount(s) paid by you to Elsevier and/or Copyright Clearance Center for denied permissions.

LIMITED LICENSE

The following terms and conditions apply only to specific license types:

15. **Translation**: This permission is granted for non-exclusive world **English** rights only unless your license was granted for translation rights. If you licensed translation rights you may only translate this content into the languages you requested. A professional translator must perform all translations and reproduce the content word for word preserving the integrity of the article.

16. **Posting licensed content on any Website**: The following terms and conditions apply as follows: Licensing material from an Elsevier journal: All content posted to the web site must maintain the copyright information line on the bottom of each image; A hyper-text must be included to the Homepage of the journal from which you are licensing at http://www.sciencedirect.com/science/journal/xxxxx or the Elsevier homepage for books at http://www.elsevier.com; Central Storage: This license does not include permission for a scanned version of the material to be stored in a central repository such as that provided by

Heron/XanEdu.
Licensing material from an Elsevier book: A hyper-text link must be included to the Elsevier homepage at http://www.elsevier.com . All content posted to the web site must maintain the copyright information line on the bottom of each image.

Posting licensed content on Electronic reserve: In addition to the above the following clauses are applicable: The web site must be password-protected and made available only to bona fide students registered on a relevant course. This permission is granted for 1 year only. You may obtain a new license for future website posting.
17. **For journal authors:** the following clauses are applicable in addition to the above:
Preprints:
A preprint is an author's own write-up of research results and analysis, it has not been peer-reviewed, nor has it had any other value added to it by a publisher (such as formatting, copyright, technical enhancement etc.).
Authors can share their preprints anywhere at any time. Preprints should not be added to or enhanced in any way in order to appear more like, or to substitute for, the final versions of articles however authors can update their preprints on arXiv or RePEc with their Accepted Author Manuscript (see below).
If accepted for publication, we encourage authors to link from the preprint to their formal publication via its DOI. Millions of researchers have access to the formal publications on ScienceDirect, and so links will help users to find, access, cite and use the best available version. Please note that Cell Press, The Lancet and some society-owned have different preprint policies. Information on these policies is available on the journal homepage.
Accepted Author Manuscripts: An accepted author manuscript is the manuscript of an article that has been accepted for publication and which typically includes author-incorporated changes suggested during submission, peer review and editor-author communications.
Authors can share their accepted author manuscript:

- immediately
  - via their non-commercial person homepage or blog
  - by updating a preprint in arXiv or RePEc with the accepted manuscript
  - via their research institute or institutional repository for internal institutional uses or as part of an invitation-only research collaboration work-group
  - directly by providing copies to their students or to research collaborators for their personal use
  - for private scholarly sharing as part of an invitation-only work group on commercial sites with which Elsevier has an agreement
- after the embargo period
  - via non-commercial hosting platforms such as their institutional repository
  - via commercial sites with which Elsevier has an agreement

In all cases accepted manuscripts should:

- link to the formal publication via its DOI
- bear a CC-BY-NC-ND license - this is easy to do
- if aggregated with other manuscripts, for example in a repository or other site, be shared in alignment with our hosting policy not be added to or enhanced in any way to appear more like, or to substitute for, the published journal article.

Published journal article (JPA): A published journal article (PJA) is the definitive final

record of published research that appears or will appear in the journal and embodies all value-adding publishing activities including peer review co-ordination, copy-editing, formatting, (if relevant) pagination and online enrichment.
Policies for sharing publishing journal articles differ for subscription and gold open access articles:
Subscription Articles: If you are an author, please share a link to your article rather than the full-text. Millions of researchers have access to the formal publications on ScienceDirect, and so links will help your users to find, access, cite, and use the best available version.
Theses and dissertations which contain embedded PJAs as part of the formal submission can be posted publicly by the awarding institution with DOI links back to the formal publications on ScienceDirect.
If you are affiliated with a library that subscribes to ScienceDirect you have additional private sharing rights for others' research accessed under that agreement. This includes use for classroom teaching and internal training at the institution (including use in course packs and courseware programs), and inclusion of the article for grant funding purposes.
Gold Open Access Articles: May be shared according to the author-selected end-user license and should contain a CrossMark logo, the end user license, and a DOI link to the formal publication on ScienceDirect.
Please refer to Elsevier's posting policy for further information.
18. **For book authors** the following clauses are applicable in addition to the above:
Authors are permitted to place a brief summary of their work online only. You are not allowed to download and post the published electronic version of your chapter, nor may you scan the printed edition to create an electronic version. **Posting to a repository:** Authors are permitted to post a summary of their chapter only in their institution's repository.
19. **Thesis/Dissertation**: If your license is for use in a thesis/dissertation your thesis may be submitted to your institution in either print or electronic form. Should your thesis be published commercially, please reapply for permission. These requirements include permission for the Library and Archives of Canada to supply single copies, on demand, of the complete thesis and include permission for Proquest/UMI to supply single copies, on demand, of the complete thesis. Should your thesis be published commercially, please reapply for permission. Theses and dissertations which contain embedded PJAs as part of the formal submission can be posted publicly by the awarding institution with DOI links back to the formal publications on ScienceDirect.

Elsevier Open Access Terms and Conditions
You can publish open access with Elsevier in hundreds of open access journals or in nearly 2000 established subscription journals that support open access publishing. Permitted third party re-use of these open access articles is defined by the author's choice of Creative Commons user license. See our open access license policy for more information.
Terms & Conditions applicable to all Open Access articles published with Elsevier:
Any reuse of the article must not represent the author as endorsing the adaptation of the article nor should the article be modified in such a way as to damage the author's honour or reputation. If any changes have been made, such changes must be clearly indicated.
The author(s) must be appropriately credited and we ask that you include the end user license and a DOI link to the formal publication on ScienceDirect.
If any part of the material to be used (for example, figures) has appeared in our publication with credit or acknowledgement to another source it is the responsibility of the user to ensure their reuse complies with the terms and conditions determined by the rights holder.
Additional Terms & Conditions applicable to each Creative Commons user license:
CC BY: The CC-BY license allows users to copy, to create extracts, abstracts and new works from the Article, to alter and revise the Article and to make commercial use of the

Article (including reuse and/or resale of the Article by commercial entities), provided the user gives appropriate credit (with a link to the formal publication through the relevant DOI), provides a link to the license, indicates if changes were made and the licensor is not represented as endorsing the use made of the work. The full details of the license are available at http://creativecommons.org/licenses/by/4.0.

CC BY NC SA: The CC BY-NC-SA license allows users to copy, to create extracts, abstracts and new works from the Article, to alter and revise the Article, provided this is not done for commercial purposes, and that the user gives appropriate credit (with a link to the formal publication through the relevant DOI), provides a link to the license, indicates if changes were made and the licensor is not represented as endorsing the use made of the work. Further, any new works must be made available on the same conditions. The full details of the license are available at http://creativecommons.org/licenses/by-nc-sa/4.0.

CC BY NC ND: The CC BY-NC-ND license allows users to copy and distribute the Article, provided this is not done for commercial purposes and further does not permit distribution of the Article if it is changed or edited in any way, and provided the user gives appropriate credit (with a link to the formal publication through the relevant DOI), provides a link to the license, and that the licensor is not represented as endorsing the use made of the work. The full details of the license are available at http://creativecommons.org/licenses/by-nc-nd/4.0.

Any commercial reuse of Open Access articles published with a CC BY NC SA or CC BY NC ND license requires permission from Elsevier and will be subject to a fee.

Commercial reuse includes:

- Associating advertising with the full text of the Article
- Charging fees for document delivery or access
- Article aggregation
- Systematic distribution via e-mail lists or share buttons

Posting or linking by commercial companies for use by customers of those companies.

20. **Other Conditions**:

v1.8

Questions? customercare@copyright.com or +1-855-239-3415 (toll free in the US) or +1-978-646-2777.